SIMULATED CLIMATOLOGY OF A GENERAL CIRCULATION MODEL WITH A HYDROLOGIC CYCLE [1]

SYUKURO MANABE, JOSEPH SMAGORINSKY, AND ROBERT F. STRICKLER

Geophysical Fluid Dynamics Laboratory, Environmental Science Services Administration, Washington, D.C.

ABSTRACT

A numerical experiment with a general circulation model with a simple hydrologic cycle is performed. The basic framework of this model is identical with that adopted for the previous study [35] except for the incorporation of a simplified hydrologic cycle which consists of the advection of water vapor by large-scale motion, evaporation from the surface, precipitation, and an artificial adjustment to simulate the process of moist convection. This adjustment is performed only when the relative humidity reaches 100 percent and the lapse rate exceeds the moist adiabatic lapse rate. The radiative flux is computed for the climatological distribution of water vapor instead of using the distribution calculated by the prognostic equation of water vapor. A completely wet surface without any heat capacity is chosen as the lower boundary. The initial conditions consist of a completely dry and isothermal atmosphere. A state of quasi-equilibrium is obtained as a result of the time integration of 187 days. A preliminary analysis of the result is performed for the 40-day period from 148th day to 187th day.

According to this analysis, the hemispheric mean of the rate of precipitation is about 1.06 m./yr. which is close to the estimate of the annual mean rainfall obtained by Budyko [5]. In the Tropics rainfall exceeds evaporation and in the subtropics the latter exceeds the former in qualitative agreement with observation. The difference between them, however, is too exaggerated, and an extremely large export of water vapor from the dry subtropics into the wet Tropics by the meridional circulation takes place. In the troposphere, relative humidity increases with decreasing altitude. In the stratosphere it is very low except at the tropical tropopause, and the mixing ratio of water vapor is extremely small in qualitative agreement with observation. Although water vapor is transported from the troposphere into the stratosphere, it is then transported toward low latitudes and condenses at the tropical tropopause where the temperature is very low and the relative humidity is high.

Based upon a harmonic analysis of the flow field and the surface pressure field, it is concluded that the effect of condensation tends to increase the wave number of the tropospheric flow and surface pressure field. Also, the incorporation of the moist process in the model seems to increase the intensity of meridional circulation in the Tropics. As a result of this increase, the transport of momentum and heat by the meridional circulation in the Tropics is much larger than that obtained from the previous study. In middle latitudes, the poleward transport of total energy in the moist-model atmosphere is less than that in the dry-model atmosphere because of the effect of the poleward transport of latent energy or the heat of condensation.

The latitudinal distributions of radiative fluxes at the top of the atmosphere and at the earth's surface coincide very well with those obtained by London [17] for the actual atmosphere. Bowen's ratio increases with increasing latitude and its magnitude coincides reasonably well with that obtained by Budyko [5] or Jacobs [11] for the ocean surface.

CONTENTS

1. INTRODUCTION

Two of the major objectives of this numerical experiment are the simulation of the hydrologic cycle and the investigation of its role in the general circulation of the atmosphere. The extensive studies of the water budget of the earth-atmosphere system (e.g., Peixoto [27] and Budyko [5]) and the careful measurements of stratospheric and upper tropospheric water vapor (e.g., Murgatroyd [21], Mastenbrook [19], and Houghton [10]) enable us to compare the results of our model with the features of the hydrologic cycle in the actual atmosphere and to discuss some of the factors essential in maintaining the moisture distribution in the atmosphere.

In the previous study [35], we performed the integration of a model without the hydrologic cycle. The stabilizing effect of moist convection, however, was incorporated in the model, i.e., the lapse rate was adjusted to the moist adiabatic lapse rate whenever it exceeded this lapse rate. In the present study, the effects of evaporation, condensation, advection of water vapor, and moist convection are incorporated in the model. The basic framework of this model is identical to the previous model except for the hydrologic cycle. Hereafter we shall call the previous model the "dry general circulation model" and the present model the "moist general circulation model" for convenience of identification. By comparing these two models, it is possible to discuss the effects of the meridional transport of latent energy and condensation on the general circulation of the atmosphere.

The basic framework of predicting large-scale precipitation was first proposed by Smagorinsky and Collins [31] and by the staff members of Tokyo University [37]. In these studies, the so-called geostrophic approximation was adopted and the effect of heat released by condensation on the large-scale flow field and temperature field was neglected. Following these studies Smagorinsky [32] has shown that an extremely large vertical motion emerges and the scale of upward motion decreases as a result of the decrease of effective static stability if one incorporates the effect of heat of condensation. According to the results of scale-analysis, such an intense vertical motion is inconsistent with the basic assumptions used for the geostrophic approximation. (See, for example, the recent comprehensive review by Phillips [28].) Also, the geostrophic model is not capable of representing the flow in low latitudes, and it completely neglects the convergence of water into the precipitation region by the ageostrophic wind component near the earth's surface. Therefore, it is necessary to use the so-called "primitive equations" for a moist model as proposed by Smagorinsky [33].

Recent numerical studies of convection performed by Lilly [16], Kasahara [12], and Ogura and Charney [23] have shown that because of convective instability, intense grid-scale convection develops exponentially in the area where the lapse rate is unstable. Since the grid-scale convection cannot be resolved by the grid itself, the computation quickly deteriorates. Therefore, it is desirable to design a scheme of convection such that the grid-scale convection does not develop. In connection with the problem of the genesis of hurricanes, Ooyama [25], Charney and Eliassen [7], and Ogura [22] proposed a system which successfully controlled the abnormal growth of hurricanes by using a concept of "balanced wind" and by cutting the direct link between vertical motion and condensation. Recently Kuo [14] and Leith [15] proposed rather sophisticated schemes of convection for studying a similar problem. However, further observational as well as theoretical studies of the macroscopic behavior of moist convection seem necessary to reach a satisfactory scheme for treating this process. In view of our ignorance in this matter, we used a very simple scheme of convective adjustment depending upon both relative humidity and the lapse rate and successfully avoided the abnormal growth of grid-scale convection. It is hoped that the results obtained by using this simple scheme can provide the basis for the computation of a more exact and better scheme of convection.

In order to avoid a sudden increase in the degrees of freedom of the model, the climatological distribution of water vapor instead of the distribution obtained from the prognostic equation of water vapor is adopted for the computation of radiative transfer only. It is our intention to eliminate this constraint in a future study.

In order to understand the role of topography and that of the distribution of land and sea, it is desirable to perform first a numerical integration of the model without these factors and to realize the importance of the missing factors by comparing the features of the model atmosphere with those of the actual atmosphere. Therefore, we adopted a completely wet and flat earth's surface without any heat capacity instead of adopting more realistic boundary conditions. The temperature of the earth's surface is determined as the balance of various thermal components such as long-wave radiation, solar radiation, sensible heat flux, and evaporation.

The next natural research step following this study is the numerical integration of a model with the actual distributions of land, sea, and mountains. It is expected that the inter-comparison among the results of the two models and the features of the actual atmosphere will greatly improve the understanding of the role of these factors in the general circulation of the atmosphere.

2. MODEL EQUATIONS

A. PROGNOSTIC EQUATIONS

The prognostic equations for temperature and the mixing ratio of water vapor on the stereographic projection are:

$$\frac{\partial(P_*T)}{\partial t} = -m^2 \left[\frac{\partial}{\partial X}\left(\frac{P_*UT}{m}\right) + \frac{\partial}{\partial Y}\left(\frac{P_*VT}{m}\right) \right]$$

$$-P_* \frac{\partial(\dot{Q}T)}{\partial Q} + \frac{R}{c_p}\frac{T\omega}{Q} + {}_HF_T + \frac{P_*}{c_p}\dot{q} \quad (2.1)$$

$$\frac{\partial(P_*r)}{\partial t}=-m^2\left[\frac{\partial}{\partial X}\left(\frac{P_*Ur}{m}\right)+\frac{\partial}{\partial Y}\left(\frac{P_*Vr}{m}\right)\right]$$

$$-P_*\frac{\partial(\dot{Q}r)}{\partial Q}+{_H}F_r+{_V}F_r-P_*C \quad (2.2)$$

where

$${_H}F_T=m^2P_*^{\kappa}\left[\frac{\partial}{\partial X}\left(P_*K_H\frac{\partial(T/P_*^{\kappa})}{\partial X}\right)+\frac{\partial}{\partial Y}\left(P_*K_H\frac{\partial(T/P_*^{\kappa})}{\partial Y}\right)\right]$$

$${_H}F_r=m^2\left[\frac{\partial}{\partial X}\left(P_*K_H\frac{\partial r}{\partial X}\right)+\frac{\partial}{\partial Y}\left(P_*K_H\frac{\partial r}{\partial Y}\right)\right] \quad (2.3)$$

$${_V}F_r=\frac{P_*}{\rho}\frac{\partial W}{\partial Z} \quad (2.4)$$

$$W=\rho K_V\frac{\partial r}{\partial Z} \quad (2.5)$$

$$\dot{q}=\dot{q}_c+\dot{q}_{RAD} \quad (2.6)$$

Since the equations of motion are identical to those used in the previous paper [35], we shall not describe them here. Following are the notations used in the equations.

- r: Mixing ratio of water vapor to dry air.
- C: Rate of change of r due to condensation.
- q_{RAD}: Rate of radiative heating.
- $\dot{q}_c$: Rate of heating due to condensation and convection.
- P_*: Surface pressure.
- t: Time.
- X: Abscissa of stereographic rectangular coordinate.
- Y: Ordinate of stereographic rectangular coordinate.
- U: Wind velocity relative to the earth in X-direction.
- V: Wind velocity relative to the earth in Y-direction.
- T: Temperature.
- Q: P/P_*, where P is pressure.
- $\dot{Q}$: dQ/dt.
- ω: dP/dt.
- R: Gas constant of air.
- c_p: Specific heat of air under constant pressure.
- K_H: Horizontal mixing coefficient as defined by equation (2B8) in previous paper [35].
- K_V: Vertical mixing coefficient as defined by equation (2B11) in previous paper [35].
- ρ: Density of air.
- m: Magnification factor of stereographic projection.
- κ: R/c_p.

For further explanation refer to previous paper [35].

B. LOWER BOUNDARY CONDITIONS

The temperature of the earth's surface T_* is determined such that it satisfies the requirement of the heat balance at the earth's surface. Because of the incorporation of the effect of evaporation, the balance equation is different from the previous study [35]. Therefore, we shall describe it here.

If we assume that the heat capacity of the earth is zero, the balance equation of heat is

$$S_*+(DLR)_*=\sigma T_*^4+({_V}H)_{Q=1}+({_V}LH)_{Q=1} \quad (2.7)$$

where S_* and $(DLR)_*$ are the net downward solar insolation and the downward long-wave radiation at the earth's surface, respectively; σ is the Stefan-Boltzman constant. The sensible heat flux at the earth's surface $({_V}H)_{Q=1}$ is

$$({_V}H)_{Q=1}=\rho(h)\cdot c_p\cdot C_D(h)\cdot|\mathbf{V}(h)|\cdot\left(T_*-\frac{T(h)}{Q^{\kappa}(h)}\right) \quad (2.8)$$

The flux of latent energy $({_V}LH)_{Q=1}$ at the earth's surface is

$$({_V}LH)_{Q=1}=\rho(h)\cdot L\cdot C_D(h)\cdot|\mathbf{V}(h)|\cdot(r_s(T_*)-r(h)) \quad (2.9)$$

where the earth's surface is assumed to be wet everywhere, L is the latent heat of evaporation, $r_s(T_*)$ is the saturation mixing ratio of water at T_*, $|\mathbf{V}(h)|$ is the magnitude of wind velocity at height h, $C_D(h)$ is the drag coefficient for the wind velocity at height h, $Q(h)$ is the Q-value at height h, and $T_*-T(h)/Q^{\kappa}(h)$ is the approximate difference between the potential temperature of the earth's surface and that at height h. For further illustrations, refer to previous paper [35].

C. RADIATIVE TRANSFER

The methods of calculating the temperature change in this study are described in detail by Manabe and Strickler [18]. A brief description of the scheme is also given in the previous paper. The distributions of gaseous absorbers and cloud used in this study are identical with those used in the previous work [35]. As we explained in the introduction, we do not use the distribution of water vapor, which is obtained from the prognostic equation of water vapor, for the computation of radiative transfer. Instead, we use the climatological distribution of water vapor as well as that of carbon dioxide, and of ozone. In short, we eliminate some part of the interaction between the hydrologic cycle and the radiative transfer. By avoiding a sudden increase in the degrees of freedom of the model this way, it is possible to compare the present result with the previous result [35] and to discuss the reasons for the differences.

3. CONDENSATION AND CONVECTION

A. NON-CONVECTIVE CONDENSATION

The rate of non-convective precipitation is computed using the following assumptions.

a. If, and only if, the relative humidity reaches 1, i.e. 100 percent, condensation may take place.

b. Relative humidity never exceeds 1, i.e., 100 percent.

c. The liquid water storage capacity of the atmosphere is zero, and all the water vapor which is condensed precipitates instantaneously.

The amount of precipitation for each time step is determined so that the requirements described above are satisfied, including the release of latent heat.

B. CONVECTIVE ADJUSTMENT

Two important processes which play a major role in the general circulation of the atmosphere are the moist and dry convection. Unfortunately, we know very little about the dynamical and thermodynamical aspects of the macroscopic behavior of moist convection. Our ignorance on this subject does not seem to warrant the incorporation of a very sophisticated scheme of the convective process at this stage of the study of the general circulation by use of a numerical model. Therefore, we used a simple convective adjustment of temperature and water vapor as a substitute for the actual convective process.

If one uses this scheme, moist convective condensation takes place only when the lapse rate tends to become super-moist-adiabatic and the relative humidity tends to exceed 100 percent. It is well known, however, that convective rainfall takes place even when the large-scale humidity is below 100 percent. Therefore, it is obvious that the simple adjustment process which we used here is insufficient for simulating the macroscopic behavior of convection in the actual atmosphere. Also, the upward transport of momentum due to free convection, which may not be negligible at all, is neglected because of our ignorance in this matter. This adjustment scheme, however, not only prevents the abnormal growth of grid-scale convection discussed in the introduction but also simulates some of the essential features of free convection in the atmosphere, i.e., 1. it prevents the appearance of a supercritical lapse rate, and 2. as a result it transfers effectively both heat and water vapor upward and causes condensation.

We shall list the basic assumptions involved in the process of convective adjustment.

(1) *Dry Convective Adjustment.*—The basic assumptions used for the dry convective adjustment are as follows:

a. When the lapse rate of an unsaturated layer tends to exceed the dry adiabatic lapse rate, the intensity of free convection is strong enough to maintain a neutral lapse rate of potential temperature.

b. The kinetic energy created by convection is dissipated and converted into heat instantaneously, i.e., the total potential energy is invariant by this adjustment.

c. The adjustment is not applied to the logarithmic boundary layer where forced convection predominates.

(2) *Moist Convective Adjustment.*—The assumptions adopted are:

a. When the lapse rate of a saturated area tends to exceed the moist adiabatic lapse rate, the intensity of free convection is strong enough to maintain a neutral lapse rate of the equivalent potential temperature.

b. The relative humidity never exceeds 1 by this moist convective process.

c. The kinetic energy of very-small-scale eddies created by this convection is dissipated instantaneously and converted into heat energy.

d. All the water condensed by this moist convective process precipitates instantaneously.

The rate of convective precipitation is determined as the consequence of satisfying all the requirements mentioned above.

C. DETAILED DESCRIPTION OF THE SCHEME

The actual computations of the amount of precipitation and the convective adjustments are performed in the following way.

(1) Compute the changes of temperature and the mixing ratio of water vapor for one time increment, Δt, neglecting the effect of condensation.

(2) Compute the distributions of relative humidity, h, and the lapse rate of temperature of the atmosphere obtained as a result of these changes.

(3) Test the relative humidity, h, and the lapse rate, γ, in the vertical column at each grid point. The adjustment to be performed as a result of the test is indicated in table 3C.

TABLE 3C.—*Test for convective adjustment*

	$h<1$			$h\geq1$	
$-\frac{\partial T}{\partial P}\leq\gamma_d$	No condensation, no convection $\delta r=0$ $\delta T=0$ (No adjustment)		$-\frac{\partial T}{\partial P}\leq\gamma_m$	Large-scale condensation only $\delta r,\ \delta T$ from $\begin{cases}r+\delta r=r_s(T+\delta T,\ P) & (3.3)\\ c_p\delta T+L\delta r=0 & (3.4)\end{cases}$	
$-\frac{\partial T}{\partial P}>\gamma_d$	Dry convection only $\delta r=0$ δT from $\begin{cases}\frac{\partial}{\partial P}\theta(T+\delta T,\ P)=0 & (3.1)\\ \frac{c_p}{g}\int_{P_B}^{P_T}\delta T dP=0 & (3.2)\end{cases}$		$-\frac{\partial T}{\partial P}>\gamma_m$	Moist convection and large-scale condensation $\delta r,\delta T$ from $\begin{cases}\frac{\partial}{\partial P}\theta_e(T+\delta T,\ r+\delta r,\ P)=0 & (3.5)\\ r+\delta r=r_s(T+\delta T,\ P) & (3.6)\\ \frac{1}{g}\int_{P_B}^{P_T}(c_p\delta T+L\delta r)dP=0 & (3.7)\end{cases}$	

γ_d—dry adiabatic lapse rate.
γ_m—moist adiabatic lapse rate.
δr—adjustment of the mixing ratio of water vapor.
δT—adjustment of the temperature.
P_T, P_B—pressure at top and base of a dry or moist unstable layer containing two or more contiguous levels of the model.

θ—potential temperature.
θ_e—equivalent-potential temperature
h—relative humidity.
r_s—saturation mixing ratio.
g—acceleration of gravity.

Further details of each adjustment are as follows.

a. *Large scale condensation only.*—At each saturated level, δr and δT of table 3C are determined from equations (3.3) and (3.4) using an iteration procedure (refer to the Appendix for details). The amount of precipitation for the entire column is computed from

$$p_{LC} = -\frac{1}{g} \int_0^{P_*} \delta r \, dP \qquad (3.8)$$

b. *Dry convection only.*—For each dry unstable layer containing n contiguous levels of the model, δT of table 3C can be computed at each level by solving the $n-1$ equations (3.1) simultaneously with equation (3.2).

c. *Moist convection and large-scale condensation.*—For each moist unstable layer containing n contiguous levels of the model, δr and δT of table 3C can be computed at each level by solving the $n-1$ equations (3.5) simultaneously with the n equations (3.6) and with equation (3.7). It is assumed that the moist adiabatic lapse rate and the value of $\partial r_s / \partial T$ at each level are unchanged by the adjustment. The procedure described in *a.*, above, is then applied to the unadjusted levels. The total precipitation for the column can then be computed from equation (3.8).

4. INITIAL CONDITIONS AND TIME INTEGRATION

The initial condition adopted for the present numerical experiment is a completely calm, dry, and isothermal atmosphere of 289° K. As we explained in the introduction, the annual mean distribution of water vapor instead of the distribution predicted by the equation of the mixing ratio of water is used for the computation of radiative transfer. The total period of integration is 187 days. In order to save computer time, the integration during the first 50 days was performed by a drastically coarse grid, ($N=5$). N is the number of grid intervals between the pole and equator. During the next 20 days the resolution of $N=10$ was adopted. After 70 days the integration was performed by use of an ($N=20$) grid.

Figure 4.1 shows the time variation of both the total potential energy and the gross static stability (refer to Appendix II of previous paper) with time. The former describes the mean temperature of the atmosphere and the latter is the indicator of the static stability of the atmosphere. The discontinuities of the curves at 50 days are caused by the sudden change of resolution from ($N=5$) grid to ($N=10$) grid. According to this figure the gross thermal structure approached a steady state at the end of the time integration. In figure 4.2 the evolution of the vertical distribution of temperature at 45° N. with time is shown. In the troposphere and upper stratosphere, where the absorption of solar radiation or heating by convection are important, the time for arriving at equilibrium is relatively short; whereas in the lower stratosphere, where both the effects of solar absorption and convection are smaller, it takes a very long time before we reach a state of equilibrium.
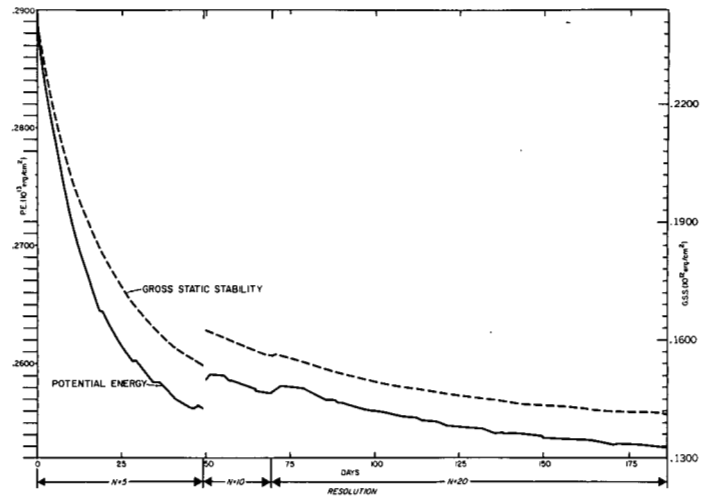

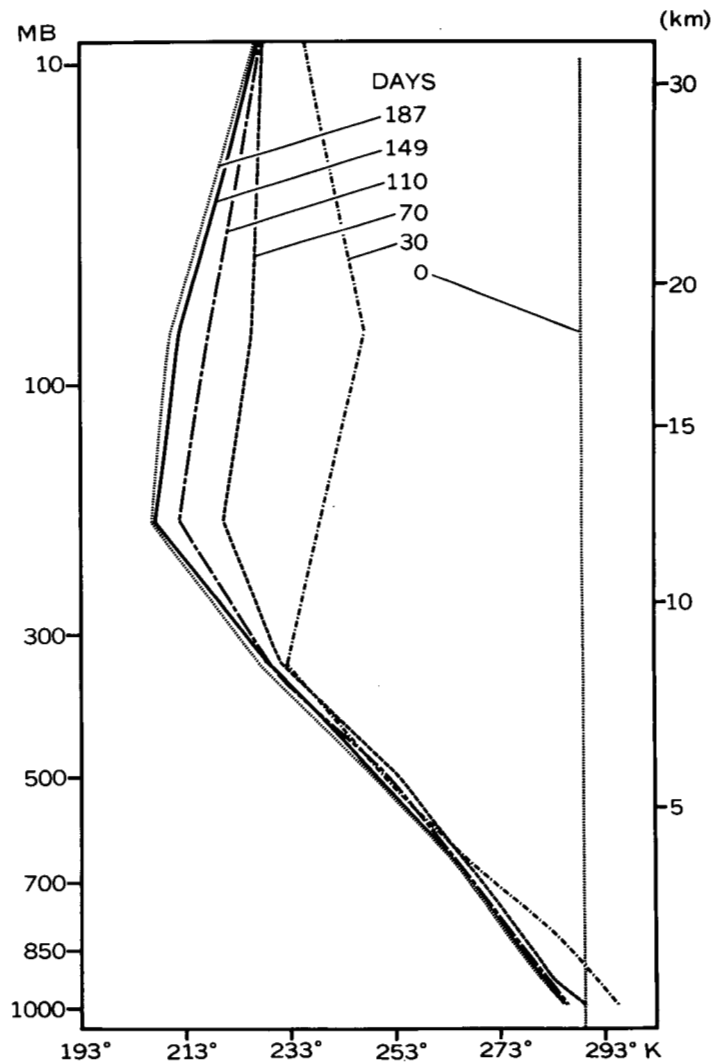FIGURE 4.1.—Variation of total potential energy and gross static stability with time.

FIGURE 4.2.—Variation of the vertical distribution of temperature of the model atmosphere with time at 45° latitude.
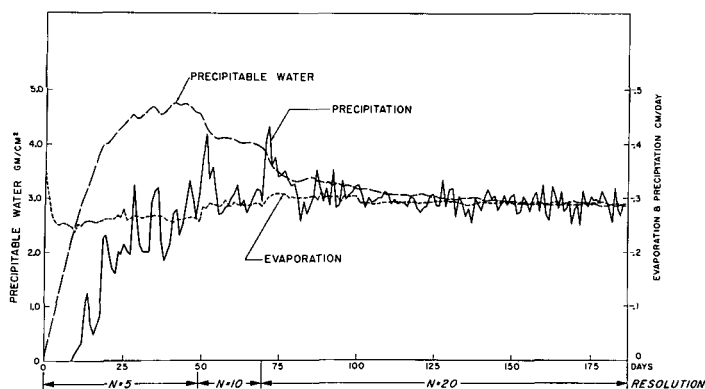
FIGURE 4.3.—Variation of the hemispheric mean of precipitable water and hemispheric rates of precipitation and evaporation with time.

Figure 4.3 shows the time variations of the hemispheric mean value of precipitable water. In the same figure the daily values of precipitation and evaporation are plotted with time. It is rather surprising that the precipitable water reached its maximum at about 40 days and started declining again. This result may be due to the fact that the atmosphere at 40 days can contain more water than in later days of integration because the temperature of the former is significantly higher than that of the latter. This curve of precipitable water almost levels off at about 150 days.

An examination of figures 4.1, 4.2, and 4.3 indicates that we reached a state sufficiently close to equilibrium except in the stratosphere where temperature still changed slowly with time. Therefore, we chose the last 40-day period (from 148th day to 187th day) for our analysis. The data are analyzed once a day and the results are averaged for this 40-day period.

5. MEAN TEMPERATURE FIELD

In figure 5.1 the latitude-height distributions of temperature that are obtained from our time integration are compared with that of the annual mean of the temperature of the actual atmosphere. In figure 5.2 a comparison is also made on the adiabatic diagram. According to these figures the agreement between the computed temperature and the observed annual mean is excellent. Since the thermal structure obtained from the dry general circulation model is also very similar to the observed distribution and discussed in the preceding paper [35], it may be preferable to discuss the present results in contrast with the previous results. In the lower half of figure 5.3 the latitudinal distributions of zonal mean temperatue at the 500-mb. level that are obtained from both the dry and moist general circulation models are compared with the observed annual mean. According to this figure, the temperature gradient in middle latitude is smaller in the present results than in the previous results. This improvement in the temperature gradient is due to a modification in the distribution of heat sources
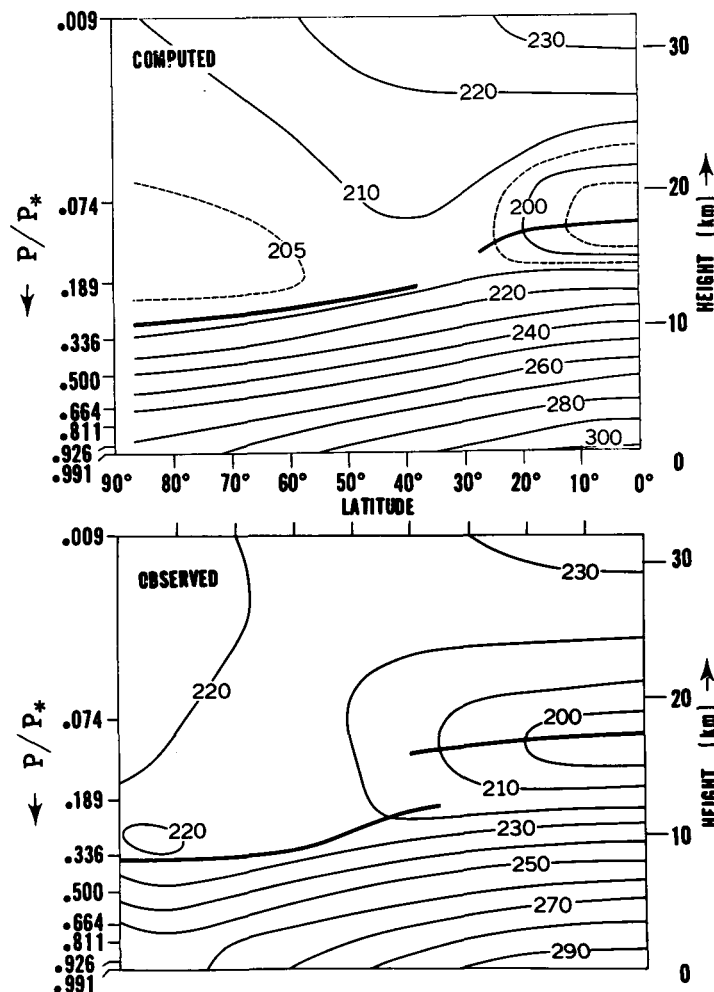

FIGURE 5.1.—In the upper   and lower part, the latitude-height distribution of temperature of the model atmosphere and that of the acutal atmosphere (Peixoto [26], Oort [24], and Kochanski [13]), are shown respectively.

resulting from the latitudinal transport of latent energy or the condensation process. For a detailed description of the distribution of heat of condensation refer to section 12.

The latitudinal distributions of temperature at level 2, $(P/P_* = 0.074)$, obtained from the dry and moist general circulation models, are compared with the annual mean of the stratospheric temperature at the 75-mb. level in the upper half of figure 5.3. The increase of temperature with increasing latitude is larger and more realistic in the present results than in the previous results. As we discussed in the previous paper, a two-cell meridional circulation predominates in our model stratosphere. The tropical cell helps maintain the latitudinal increase of temperature in low latitudes, whereas the polar cell tends to destroy the relatively warm area created by the large-scale eddies in high latitudes. According to the comparison between the distributions of the zonal mean of vertical motion of the moist and dry general circulation models, the intensity of the polar cell at the second stratospheric level is much weaker for the moist
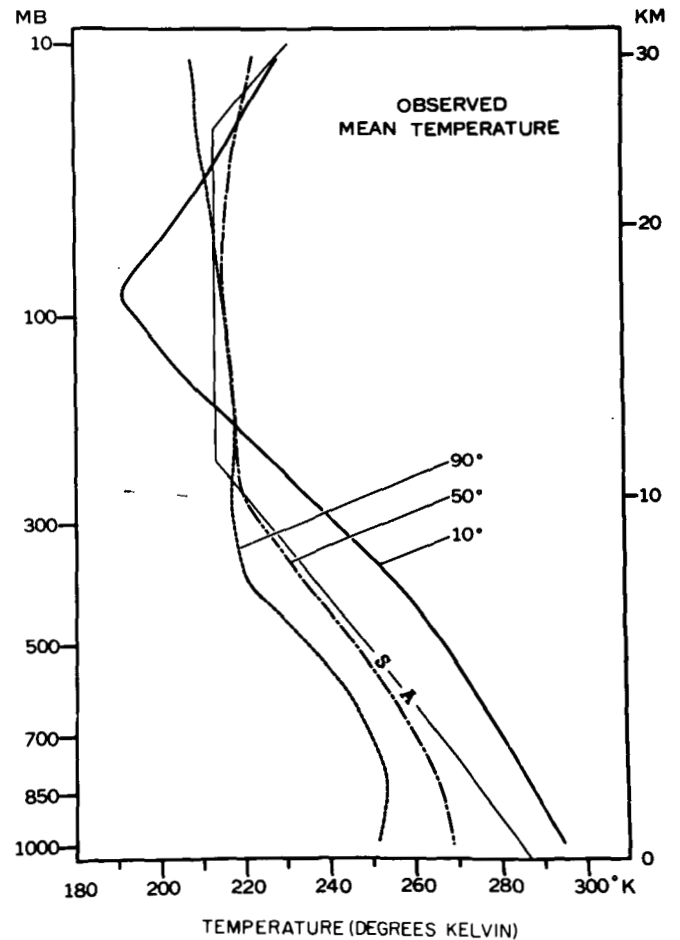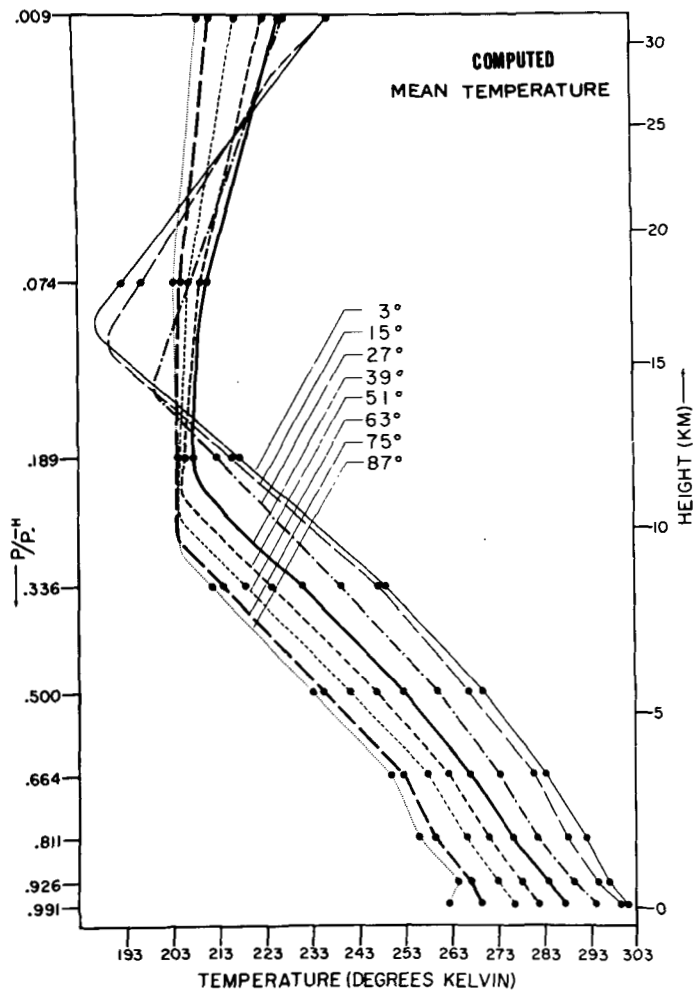
FIGURE 5.2.—In the left and right hand sides of the figure are shown the vertical distribution of computed and observed temperature at various latitudes.

model than for the dry model, and the tropical cell in the stratosphere of the moist model is almost as strong as that of the dry model. (Refer to figure 6.3 of this paper and figure 4B2 of previous paper.)

Therefore, the increase of stratospheric temperature with increasing latitude is somewhat larger for the moist model atmosphere than for the dry model atmosphere. The temperature change due to the heat transport by the large-scale eddies tends to decrease the latitudinal increase of stratospheric temperature in low latitudes (0°~35°) as figure 5D6 of the previous paper [35] shows. This tendency is less pronounced in the moist model atmosphere than in the dry model atmosphere (see fig. 5D3 of previous paper and fig. 12C4 in sec. 12). This difference is partly responsible for the difference in the latitudinal increase of stratospheric temperature in the low latitudes. For a definitive evaluation of the effect of condensation on the distribution of stratospheric temperature, it seems to be necessary to wait until a quantitatively successful simulation of the tropospheric hydrologic cycle is accomplished.

6. MEAN FLOW FIELD

Figure 6.1 shows the latitude-height distribution of the zonal mean of the zonal wind which emerged as a result of the time integration. In the same figure the distribution of the annual mean of zonal wind based upon data by Buch [4], Starr and White [38], and Oort [24], and the distributions of zonal wind during winter and summer obtained by Kochanski [13] are shown for comparison. The characteristic features of the present results are as follows:

(1) The subtropical jet stream is very intense and is located in very low latitudes (25° N.).

(2) In the stratosphere, the axis of the maximum zonal current tilts sharply, i.e., the latitude of maximum wind increases with increasing altitude.

(3) A very weak easterly current appears in the upper stratosphere of the Tropics.

(4) A surface easterly current appears at about 60° N. instead of in the polar region.

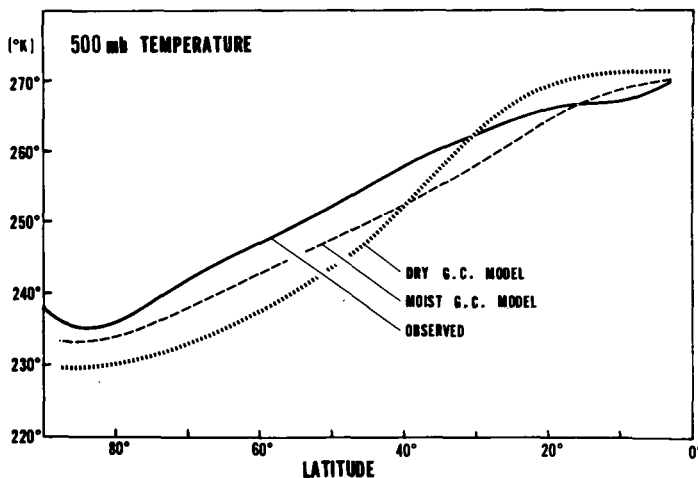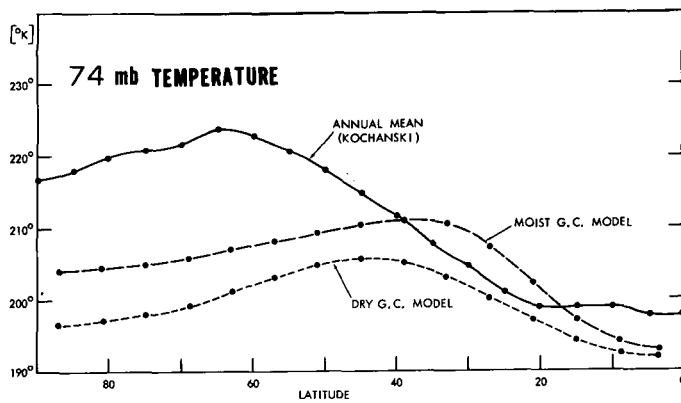The general features of our results are closer to those of

FIGURE 5.3—The latitudinal distribution of observed annual mean temperature and computed temperature at different levels of the atmosphere. The observed distributions at the 74-mb. and at the 500-mb. levels are obtained from the results of Kochanski [13] and Peixoto [26] respectively.

the zonal wind during winter than to those of the annual mean, though the modes of the computed distribution deviate to the south of those of the actual winter atmosphere.

In figure 6.2 the latitudinal distributions of the zonal mean of the zonal wind at the stratosphere (level $k=2$, $P/P_*=0.074$) which are obtained from both the dry and moist general circulation models, are compared with the annual mean distribution of the actual atmosphere at the 75-mb. level. In middle latitudes the intensity of zonal wind obtained from our present computation is significantly weaker than that which is obtained from the dry general circulation model. This improvement is consistent with the improvement of the temperature gradient in middle latitudes that we discussed in section 5.

Figure 6.3 shows the latitude-height distribution of zonal mean vertical velocity. According to our comparison between the present distribution and the results obtained from the integration of the dry model, the following features of the present results are noteworthy.

(1) The upward-moving branch of the tropical cell is very intense and narrow, and the downward-moving branch in the subtropics is wide.

(2) The intensity of the cell in middle latitudes is weaker than in the previous result.

The effects of the process of condensation on the meridional circulation described above seem to be reasonable qualitatively, but they may be exaggerated. This powerful tropical cell causes a large equatorward transport of latent energy and accordingly a very drastic tropical rain belt, as we shall describe later. Because of the complexity of the model, it is rather difficult to determine the reason such an intense meridional circulation emerges. We shall speculate on this problem later.

7. MEAN MOISTURE FIELD

Figure 7.1 shows the vertical distribution of the hemispheric mean of the mixing ratio of water vapor obtained as a result of integration. Based upon the data compiled by Peixoto [27] by using radiosonde measurements, the hemispheric mean values for the lower troposphere are computed and plotted in the same figure. For the upper troposphere the average mixing ratios for the latitude range of 0°–70°N. are computed from the results obtained by Murgatroyd [21] from aircraft measurements, and are added to the same figure. There have been many results which suggest the increase of water vapor with increasing altitude in the stratosphere. After a careful examination of his results, Mastenbrook [19] finally concluded that the increase is due to contamination from the balloon itself and that the stratosphere is very dry indeed. Two of his measurements are added to the figure after slight smoothing of his original data. The recent measurements performed by Houghton [10] using the infrared spectrometer also suggest the existence of a dry stratosphere. According to this comparison, the computed results are in reasonable agreement both in the troposphere and in the stratosphere. The formation of a dry stratosphere in our model is very encouraging. We shall examine the stratospheric water budget in section 10.

In the upper troposphere the coincidence between our results and the distribution of the area mean of the mixing ratio obtained by Murgatroyd is remarkable. Near the earth's surface the computed mixing ratio is significantly larger than the observed partly because of the assumption of a completely wet surface. As a result of this discrepancy the computed amount of precipitable water is significantly larger than the observed amount. As figure 7.2 shows, the computed precipitable water is as large as the observed precipitable water for summer although the general features of the computed latitudinal distribution compare favorably with the observed except in the Tropics where the computed values sharply increase with decreasing latitude.

The latitude-height distribution of relative humidity obtained from our computation and that of the actual atmosphere for the summer season are shown in the upper
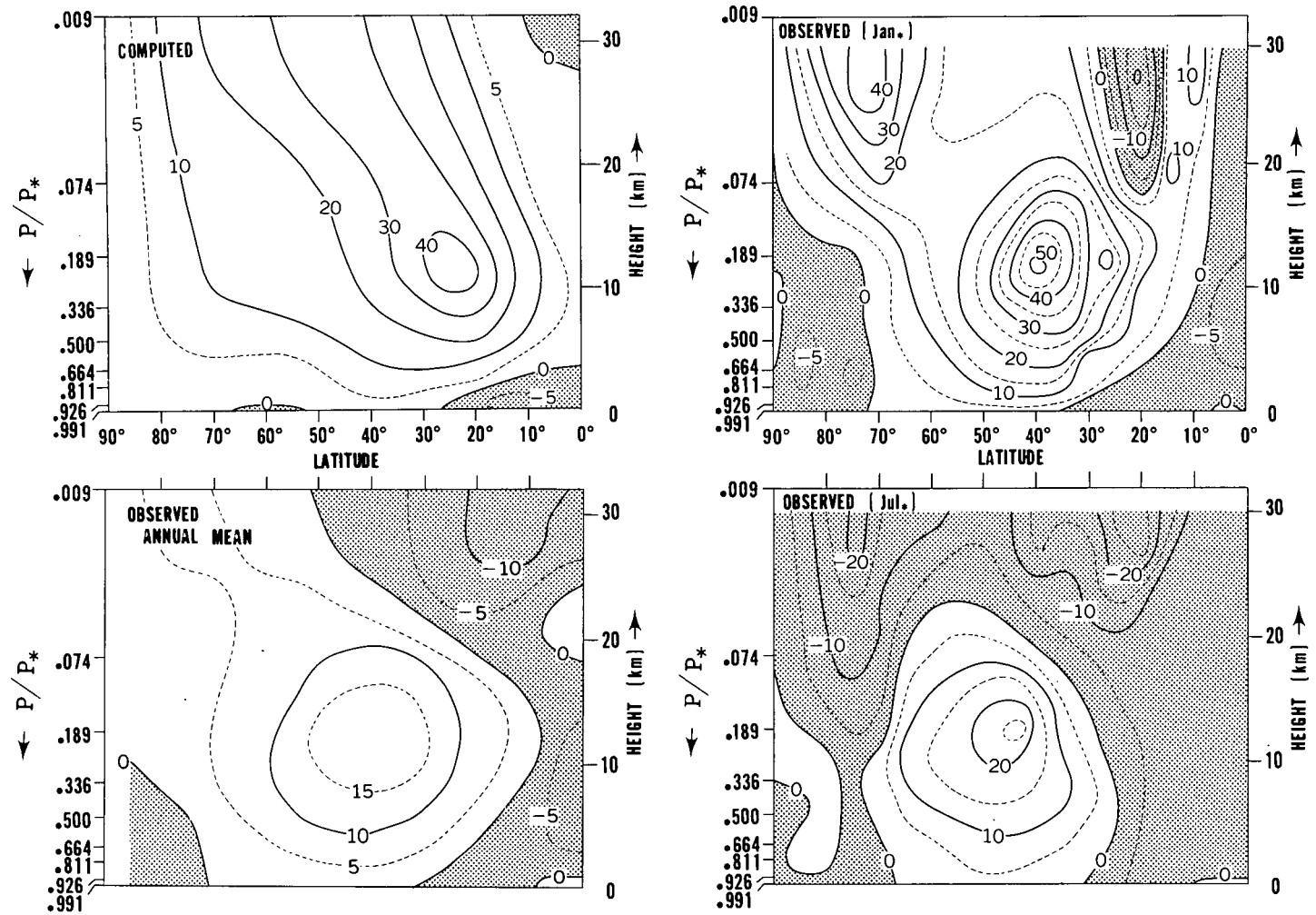
FIGURE 6.1.—Latitude-height distribution of the zonal mean of the zonal wind. The computed distribution and the observed annual mean, which is obtained from the results of Buch [4], Oort [24], are shown in the upper left and lower left, respectively. The distributions at 80° W. obtained by Kochanski [13] for both January and July are shown on the right-hand side of the figure.
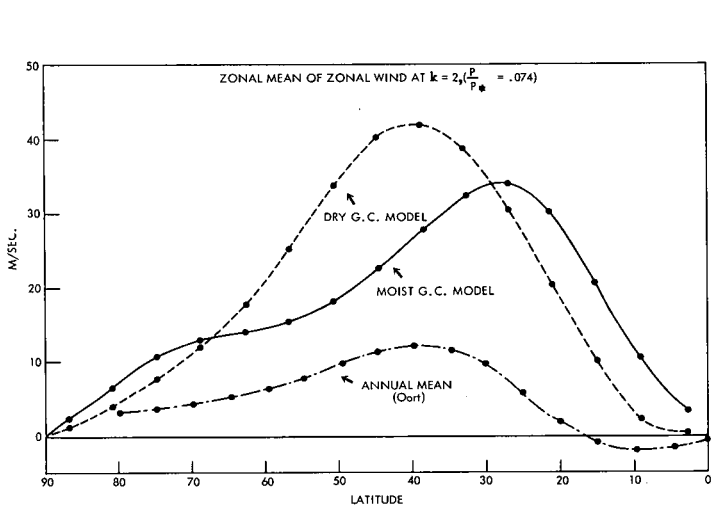

FIGURE 6.2.—Latitudinal distribution of the zonal mean of the zonal wind at the 2d model level $(P/P_* = 0.074)$ are shown together with that at the 75-mb. level of the actual atmosphere obtained from the results of Oort [24].
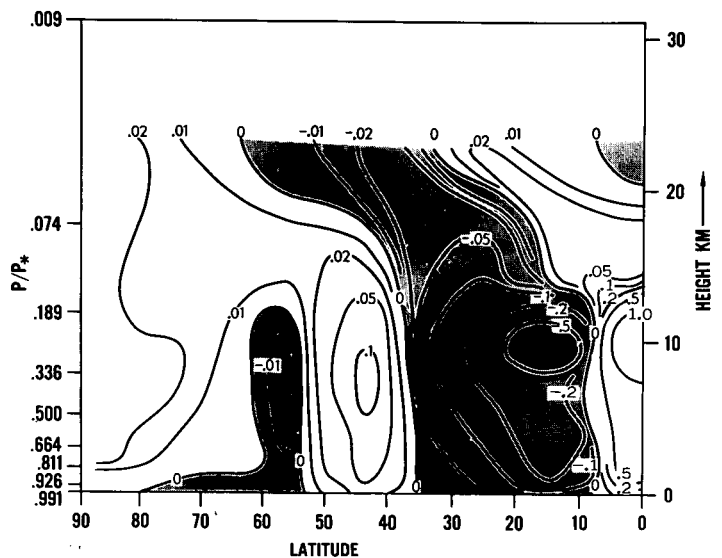
FIGURE 6.3.—The latitude-height distribution of vertical component of wind of the model atmosphere. Units are cm./sec.
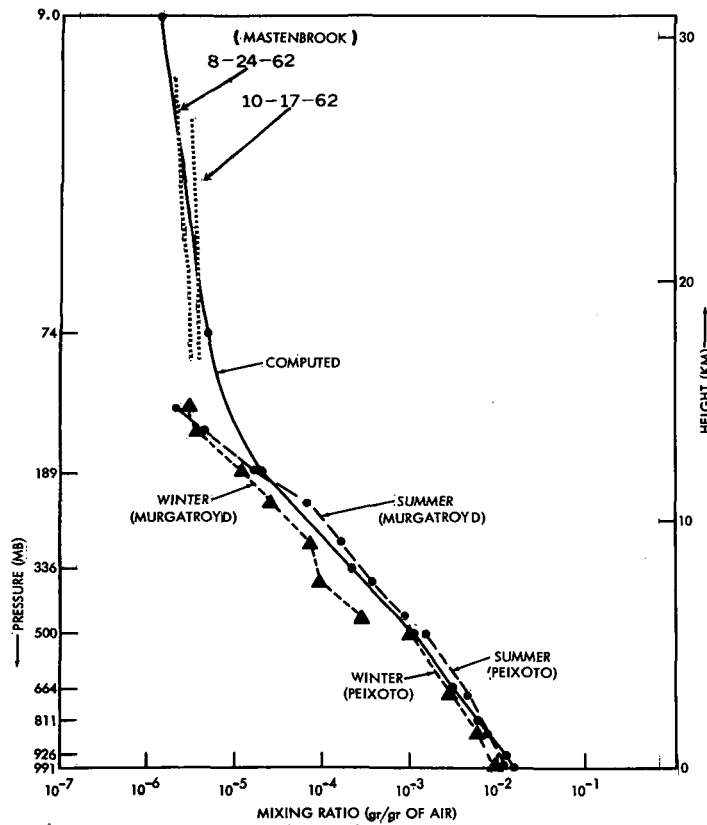
FIGURE 7.1.—The vertical distributions of the hemispheric mean of the mixing ratio of water vapor for the computed and the actual atmosphere. Data obtained by Mastenbrook [19], Murgatroyd [21] and Peixoto [27] are used.
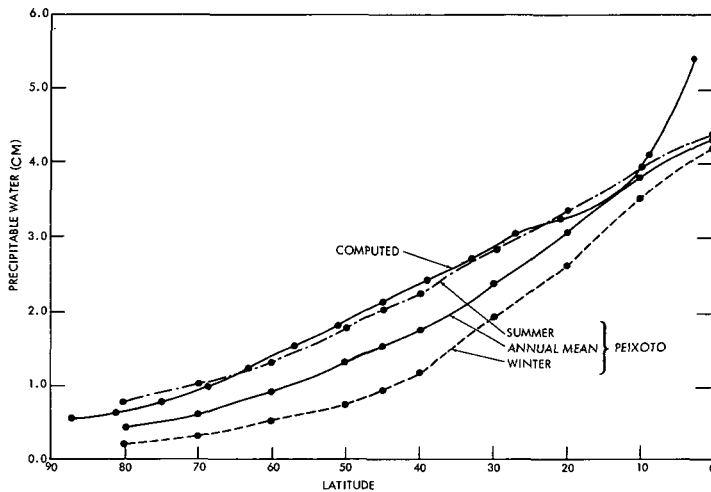

FIGURE 7.2.—Latitudinal distributions of precipitable water (cm.) contained in the model atmosphere and in the actual atmosphere. Observed distributions for summer, winter, and the annual mean are taken from the results of Peixoto [27].
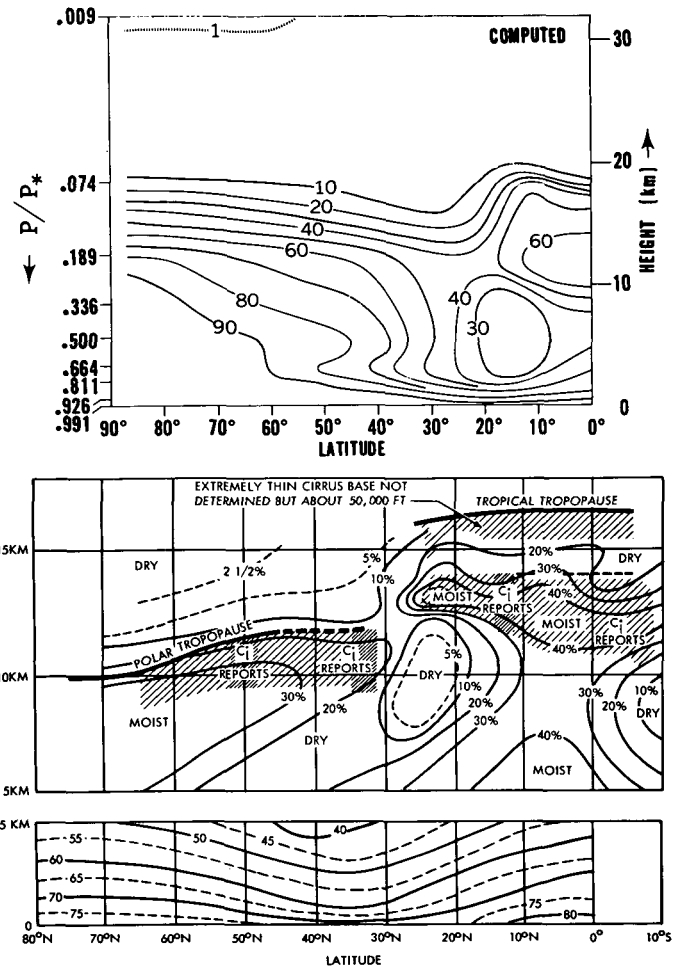

FIGURE 7.3.—In the upper part of the figure, the latitude-height distribution of relative humidity (in percent) of the model atmosphere is shown. In the lower part is shown that of the actual atmosphere for summer season (by Murgatroyd [21], Telegadas and London [39]).

we have the relative humidity data of Murgatroyd [21]. There are many qualitative features which are common to both the computed and observed atmospheres. For example, the very dry stratosphere, the wet lower troposphere, and the dry subtropics are common. In the upper troposphere in the Tropics, a relatively moist region emerges in qualitative agreement with the observation by Murgatroyd [21]. This moist region is partly attributable to stronger radiative cooling at this level. Since the data compiled by Murgatroyd are based upon relatively few observations (except those performed over England), an exact quantitative comparison for the upper tropospheric region is not justified. The distributions obtained by Telegadas and London [39], on the other hand were compiled from many routine radiosonde observations. According to our comparison, the relative humidity near the earth's surface obtained from our computation is higher than that of the actual atmosphere. As we pointed out, this discrepancy is partly due to the assumption of a wet surface adopted for the present computation. However, there may be other reasons for this difference because
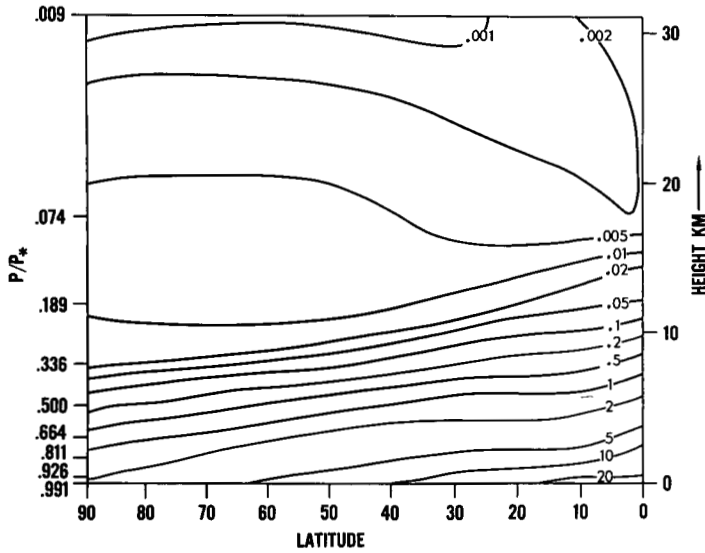
and lower parts of figure 7.3, respectively. The distribution of observed relative humidity in the lower troposphere was compiled by Telegadas and London [39] using radiosonde observations, and that in the upper troposphere was constructed by Murgatroyd [21] using aircraft observations. The reason we show the observed distribution for summer is that this is the only season for which

FIGURE 7.4.—The latitude-height distribution of the mixing ratio of water vapor in the model atmosphere. Units are gm./kg. of air.

$$\phi, \ \frac{P}{\overline{P}_*^H} = .500$$

FIGURE 8.1—Solid lines show the contour lines of the geopotential and dashed lines show those of the temperature on the isobaric surface of $P/\overline{P}_*^H = 0.5$. (175th day of integration.)

the computed humidity is about 95 percent and higher than the mean relative humidity on the ocean surface which is about 80 percent.

One possible reason is the shortcoming of the moist-convective adjustment. According to the present scheme, moist convection takes place only when the lapse rate becomes superadiabatic and the relative humidity reaches 100 percent, whereas in the actual atmosphere, moist convective condensation is usually observed when the large-scale distribution of humidity is much less than 100 percent. Therefore, it is probable that the improvement of the criterion for the convective adjustment would increase the upward transport of water vapor due to the adjustment and, accordingly, improve the distribution of relative humidity in the model atmosphere.

Another discrepancy is the appearance of a very humid region around the pole. This is caused by the upward branch of meridional circulation in the polar region where downward motion appears in the actual atmosphere. Also, the latitude of the subtropical dry belt obtained from our model is too low. Refer to figure 10B1 which shows the latitudinal distribution of evaporation and that of precipitation. According to this figure the latitudinal width of the tropical rain belt is very small and consequently the dry belt is also located at too low a latitude.

Finally, the latitude-height distribution of the mixing ratio of air obtained as a result of the numerical integration is shown in figure 7.4. As we mentioned, the mixing ratio is very small in the stratosphere. The mixing ratio of the tropical tropopause is about 3×10^{-6} gm./gm. of air and increases with increasing latitude up to 60° N. In high latitudes, the mixing ratio in the stratosphere ($k=2$, $P/P_*=0.074$) is about 7×10^{-6} gm./gm. of air. These values are not far from those obtained by Mastenbrook [19], Murgatroyd [21], and Houghton [10] in this region of the actual atmosphere.
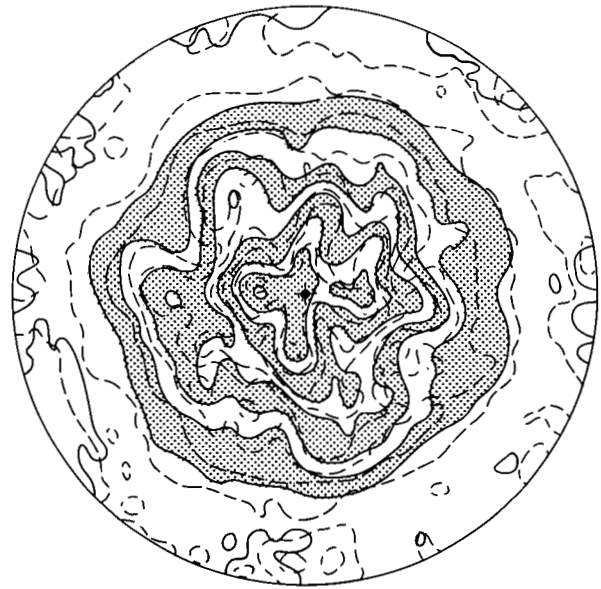
In the upper stratosphere the computed mixing ratio is 0.7–2.0×10^{-6} gm./gm. of air and is very dry.

8. SYNOPTIC MANIFESTATION

In figure 8.1 an example of the map of the geopotential height and temperature of the 500-mb. surface is shown, and in figure 8.2 the map of surface pressure obtained from the present experiment is compared with that obtained from the dry general circulation model. According to this figure, the scale of the pressure field obtained from the moist general circulation model is significantly smaller than that obtained from the dry general circulation model. In other words, the heat of condensation tends to decrease the scale of the pressure field at the earth's surface and to increase the total number of Lows in the hemisphere. Note the clusters of small Lows that appear in figure 8.2. They remind us of a cyclone family in the actual atmosphere. An increase of resolution of the model seems to be highly desirable to resolve and describe sufficiently the pressure distribution accompanying the cyclone family or front.

Figure 8.3 shows the vertical distributions of the hemispheric mean of the effective wave number $\bar{n}$ which is defined by the following equation

$$\bar{n} = (\int n \cdot dE(n))/\int dE(n)$$

where $E(n)$ denotes the energy spectrum. In the same figure, the corresponding distributions obtained from the dry model are shown.

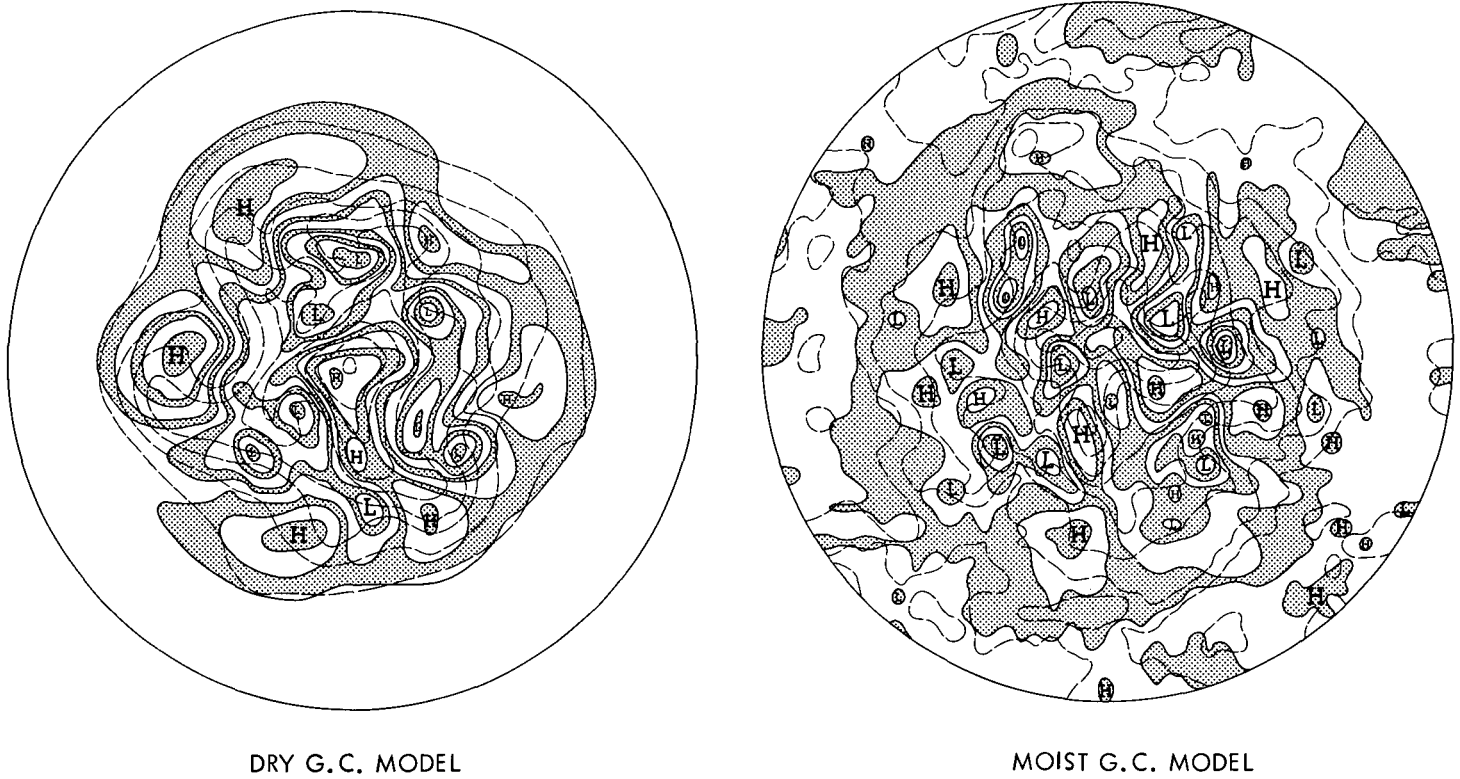DRY G.C. MODEL   MOIST G.C. MODEL

FIGURE 8.2—Contour lines of surface pressure obtained from the moist general circulation model (175th day) and those obtained from the dry general circulation model (259th day) are shown in the right- and left-hand side of the figure (every 5 mb.) respectively. Dashed lines show the isotherms on the earth's surface (every 5° C.).
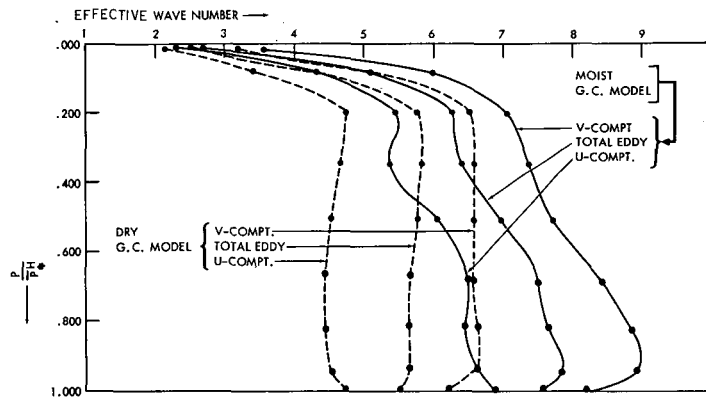

FIGURE 8.3.—The vertical distributions of the hemispheric mean of the effective wave number of eddies for both dry and moist general circulation models. The distributions of the meridional component of wind, of zonal component of wind, and of both components are shown together.
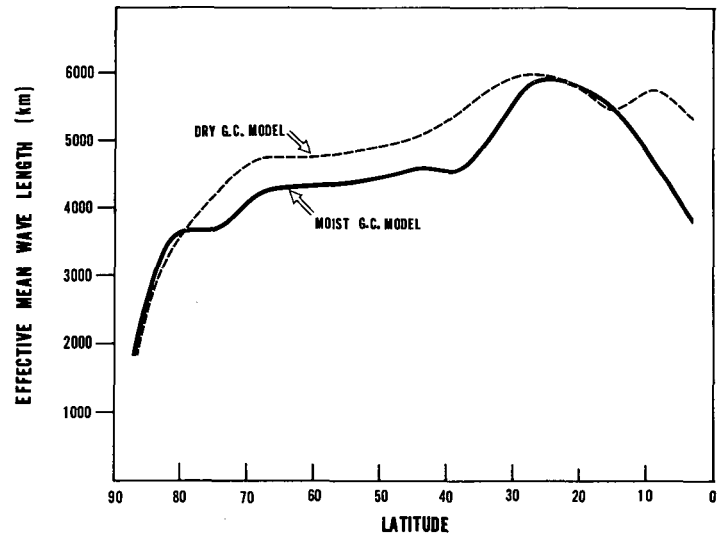

FIGURE 8.4.—Latitudinal distributions of the pressure-weighted vertical mean of the effective wavelength ($2\pi a \cos \theta/\bar{n}$, where θ is latitude and a the radius of the earth) for both the moist and the dry atmosphere.

According to this comparison the wave number of the moist model is significantly larger than that of the dry model and increases with decreasing altitude in the troposphere except very near the earth's surface. The level of maximum wave number is very close to the earth's surface and is at about the 900-mb. level. Since the latitudinal distribution of eddy kinetic energy in the moist model atmosphere is much larger than that of the dry model atmosphere in the Tropics where the wave number is large (see fig. 9.3), the comparison between the

hemispheric mean wave numbers exaggerates the difference. Therefore, figure 8.4, which shows the latitudinal distributions of the effective wavelength ($=2\pi a \cos\theta/\bar{n}$) for both the moist and dry model atmospheres, is made. According to this figure the effective wavelength of the moist atmosphere is shorter than that of the dry atmosphere except in the subtropics and very high latitudes
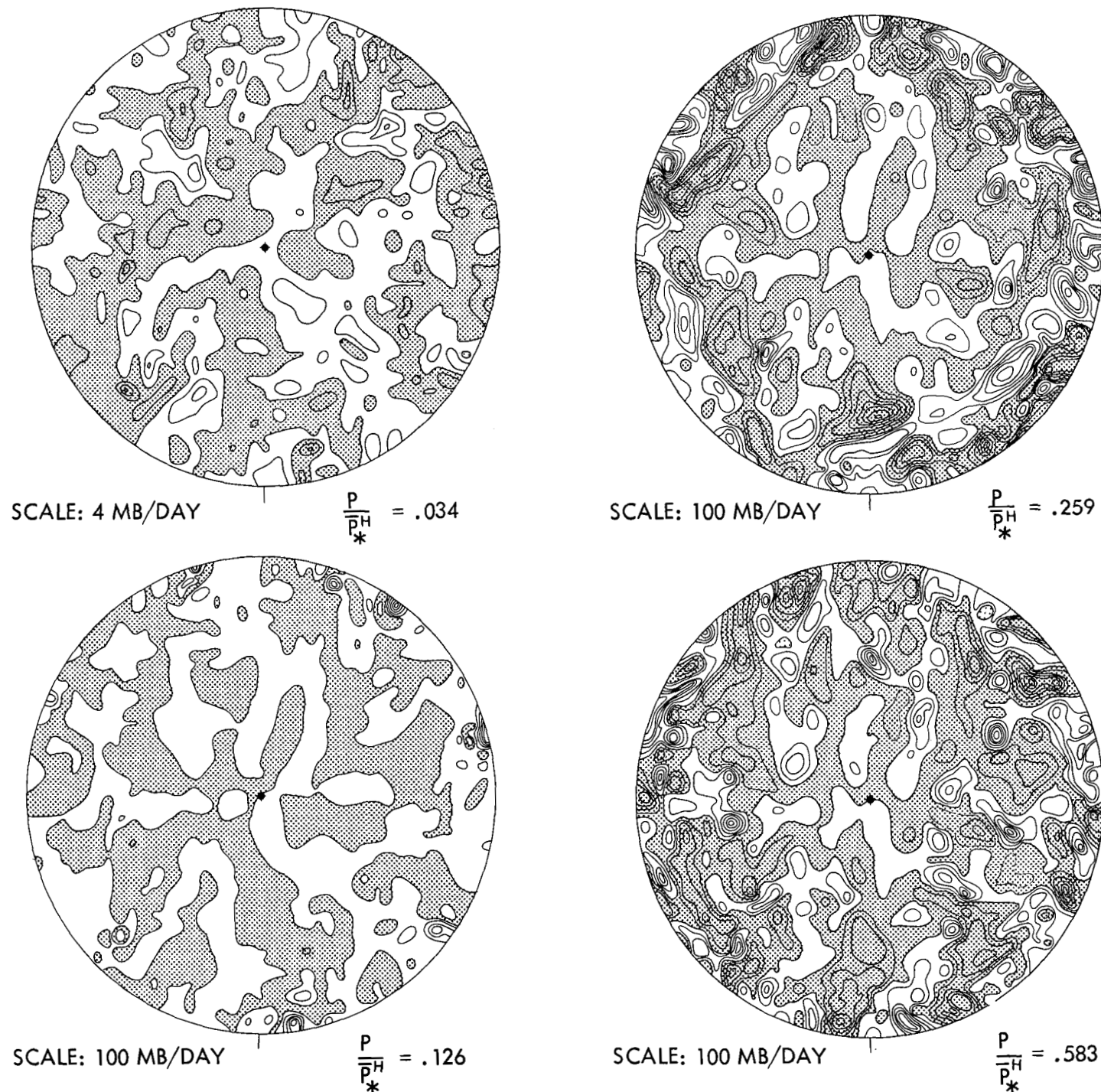
SCALE: 4 MB/DAY $\dfrac{P}{P_*^H} = .034$

SCALE: 100 MB/DAY $\dfrac{P}{P_*^H} = .259$

SCALE: 100 MB/DAY $\dfrac{P}{P_*^H} = .126$

SCALE: 100 MB/DAY $\dfrac{P}{P_*^H} = .583$

FIGURE 8.5.—Isolines of vertical P-velocity $(P_* \cdot \dot{Q})$ on 175th day of the time integration at $P/P_*=0.034$, 0.126, 0.259, and 0.583. The areas of positive $\dot{Q}$ (downward motion) are shaded. Note, the interval of isolines is not common for all levels.

where the rate of condensation is very small. These results show that the heat released by condensation tends to produce small-scale motions, and is consistent with the effect of condensation on the surface pressure system which we described in the previous paragraph.

Figure 8.5 shows the maps of the distribution of the vertical P-velocity $(=P_* \cdot \dot{Q})$ at $P/P_*=0.034, 0.126, 0.259$, and 0.583 at the 175th day of integration. Note that the intervals of the isolines adopted for these maps are not the

same. According to the comparison between the distribution of vertical P-velocity at $P/P_*=0.583$ in this figure and that of the previous study [35] (see fig. 8.5a), the tropospheric vertical P-velocity obtained from the moist model has much stronger and smaller centers of upward motion in lower latitudes than does the dry model. In middle latitudes, the difference is not so pronounced. Figure 8.6 shows examples of the longitudinal distribution of vertical P-velocity at 41.5° N. for both the moist and
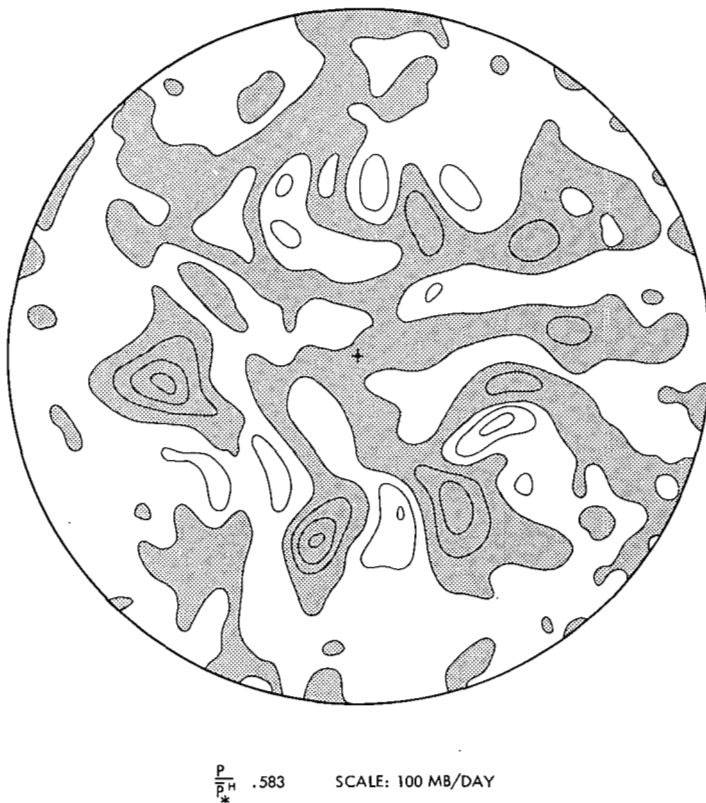
$$\frac{P}{P_*^H} \quad .583 \qquad \text{SCALE: 100 MB/DAY}$$

FIGURE 8.5a.—Isolines of vertical P-velocity $(P_* \dot{Q} \cdot)$ at $P/P_* = 0.583$ which is transferred from figure 4C5 of previous paper [35].

FIGURE 8.6.—Longitudinal distributions of vertical P-velocity at various levels. Distributions on the 259th day in the dry atmosphere and those on the 175th day in the moist atmosphere are shown on the left- and the right-hand side of the figure, respectively.

dry atmospheres. This figure shows that the scale of vertical motion obtained from the moist model is somewhat smaller than that of the dry model because of the effect of heat released by condensation.

Figure 8.7 shows the map of relative humidity at $P/P_* = 0.074$, 0.811, 0.926, and 0.991 on the 175th day. As we discussed in section 7, the computed relative humidity generally increases with decreasing altitude. The variability of the tropospheric relative humidity, on the other hand, increases with increasing altitude. The qualitative features of this result coincide with the observed features of relative humidity in the atmosphere, particularly over the ocean. The relative humidity of the lowest level $(k=9, P/P_* = 0.991)$, however, is too high. In the second stratospheric level, $(k=2, P/P_* = 0.074)$, the relative humidity is low in most of the hemisphere, but in the Tropics it has a large variability suggesting the influence of penetrative convection to this level. We did not prepare a map for the first stratospheric level $(k=1, P/P_* = 0.009)$. At this level the relative humidity is around 1 percent or less. (See fig. 7.3.)

Since the scale of the pattern of relative humidity and that of vertical motion in the troposphere are very small, it is clear that the resolution adopted for our present calculation is not sufficient. The increase of resolution, therefore, could alter our result significantly.
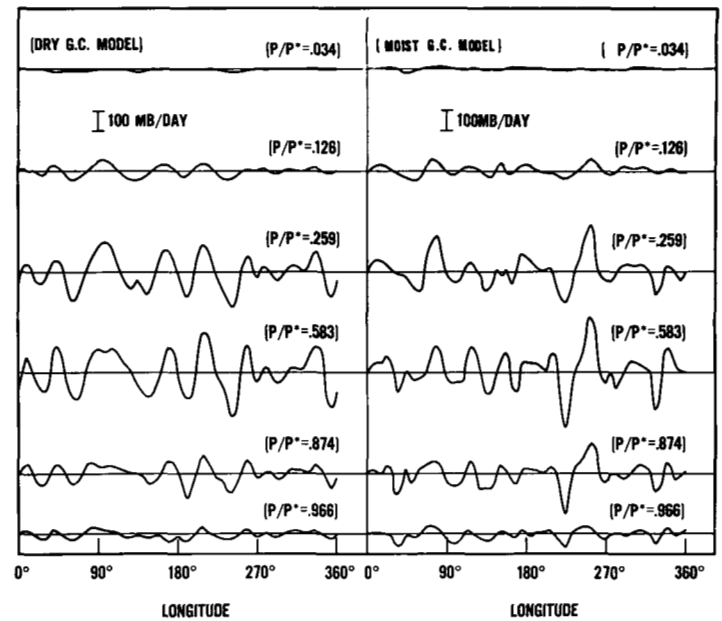
9. KINETIC ENERGY FIELD

Figure 9.1 shows the time variation of the latitudinal distribution of zonal kinetic energy obtained from the time integration. The maximum of the zonal kinetic energy corresponding to the subtropical jet stream is very large and is located at too low a latitude (refer to fig. 6.1). It is noteworthy that a secondary maximum of the zonal kinetic energy appears at about 60° N. during a certain period. This feature did not appear in the dry model atmosphere (see fig. 4E4 of the previous paper [35]) and reminds us of the double maximum of zonal current which occurs in the actual atmosphere during certain periods of winter.

The latitude-height distribution of eddy kinetic energy obtained from the present computation is shown in figure 9.2. The level of maximum eddy kinetic energy is located at the third model level $(P/P_* = 0.189)$ as it was in the previous result and coincides with the level of the observed maximum. This distribution, however, is quite different from that obtained from the previous study [35]. In figure 9.3, the latitudinal distributions of eddy kinetic energy of both the dry and the moist general circulation models at the 500-mb. level are compared with that of the actual atmosphere obtained by Saltzman [30]. Based upon this figure we may make the following comments:

1. Observed eddy kinetic energy in middle latitudes is larger than the eddy kinetic energy obtained from either the dry or moist model.

2. The eddy kinetic energy in middle latitudes is smaller for the present results than for the previous results.
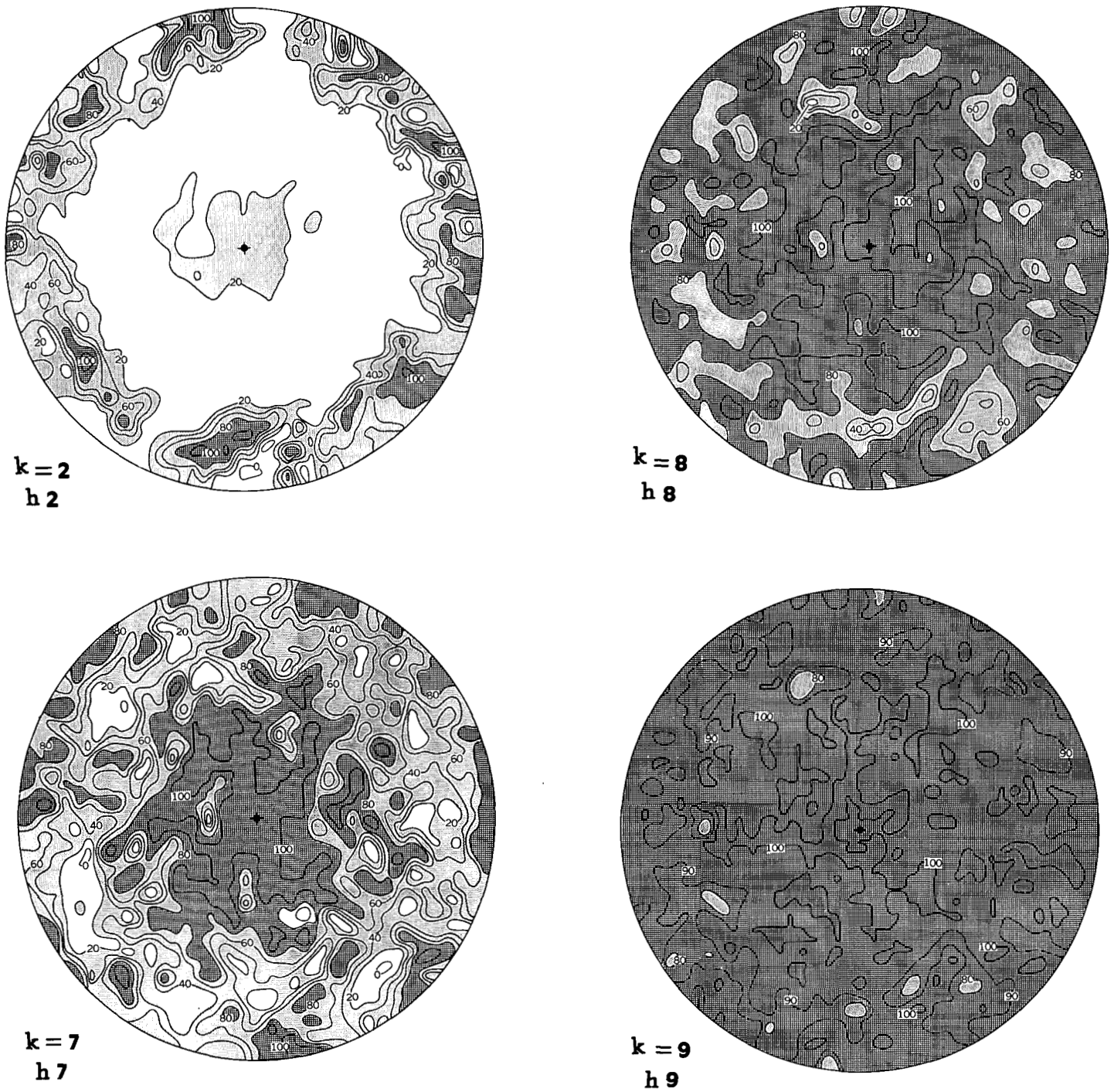
FIGURE 8.7.—The map distributions of the relative humidity on 175th day at $P/P_* = 0.074$, 0.811, 0.926 and 0.991. Dark shade, 80–100 percent; medium shade, 20–80 percent; blank area, 0–20 percent.

3. The distribution of the eddy kinetic energy obtained from the present moist general circulation model has two maxima; one in the middle latitudes, and the other in the Tropics.

There are various possible reasons why in the middle and high latitudes the eddy kinetic energy of the actual atmosphere is larger than that obtained from our numerical integration. As we pointed out in the previous

study [35], the lack of land and sea or mountains in our model may be one of the reasons for this discrepancy. According to our experience, the increase of the effective eddy Reynolds number resulting from further increase of resolution also increases the eddy kinetic energy. (Note that the horizontal mixing coefficient of the model is dependent upon the grid size.)

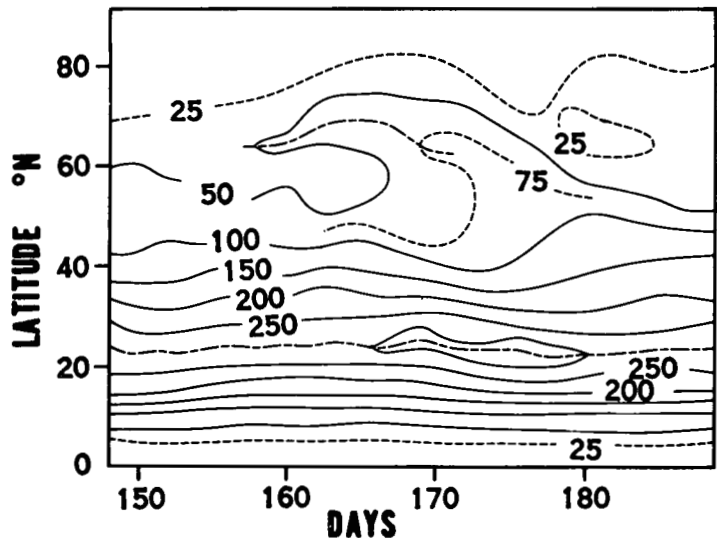The reason the eddy kinetic energy obtained from the

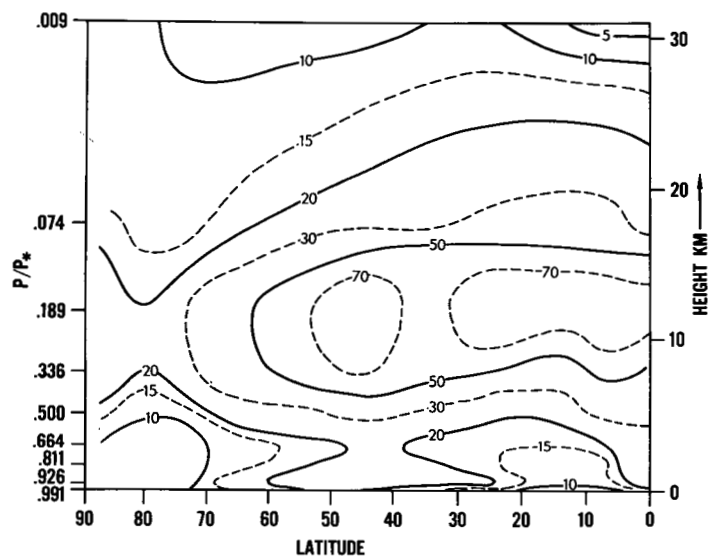FIGURE 9.1.—The variation of the latitudinal distribution of zonal kinetic energy with time. Unit is joule cm.$^{-2}$

FIGURE 9.2.—The latitude-height distribution of eddy kinetic energy in the model atmosphere. Unit is 10^{-3} joule cm.$^{-2}$ mb.$^{-1}$

FIGURE 9.3.—The latitudinal distributions of eddy kinetic energy at the 5th model level $(P/P_* = 0.5)$ of both the dry and moist general circulation models and that at 500-mb. level of the actual atmosphere obtained by Saltzman [30].

FIGURE 9.4.—The latitudinal distributions of source $(-\overline{\mathbf{V} \cdot \boldsymbol{\nabla}\phi}^H)$ and sink $(\overline{\mathbf{V} \cdot \mathbf{F}}^H)$ of kinetic energy in the model atmosphere.

moist model is smaller than that obtained from the dry model in middle latitudes may be the difference in the degree of baroclinic instability caused by the difference in the vertical wind shear. According to the comparison between the vertical eddy flux of heat in the moist model atmosphere and that in the dry model atmosphere, the former is significantly smaller than the latter in middle latitudes. (See the upper part of fig. 5D4 of the previous paper [35] and the lower part of fig. 12C4 of this paper.) This result implies that the release of potential energy in the moist model atmosphere is smaller than that in the dry model atmosphere in middle latitudes. Therefore, the eddy kinetic energy of the former is smaller than that of the latter in middle latitudes.
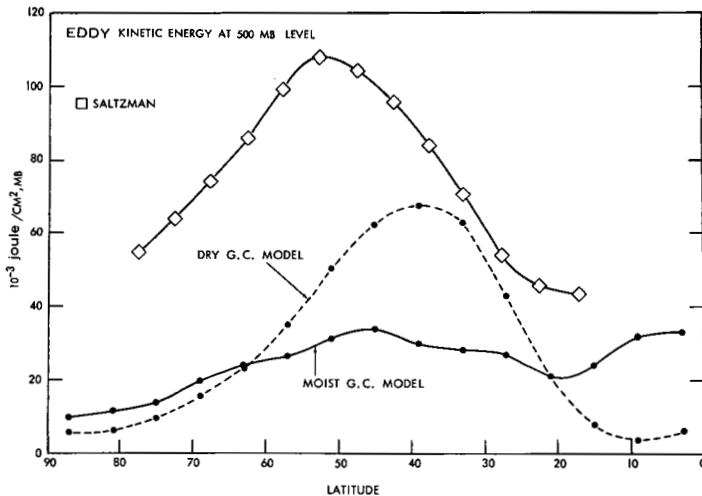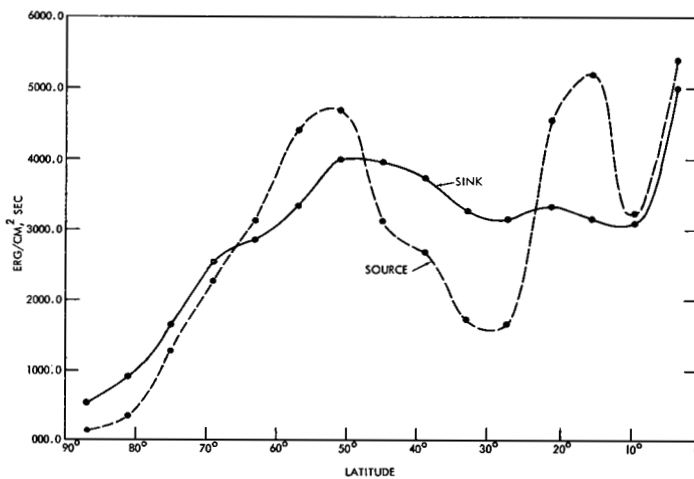
The tropical maximum of eddy kinetic energy obtained from the present study is produced by the release of available potential energy generated by the heat released by condensation in the Tropics. According to figure 12C4, the potential energy is released in the Tropics as well as in middle latitudes. Figure 9.4 shows the latitudinal distribution of the source $(-\overline{\mathbf{V} \cdot \boldsymbol{\nabla}\phi}^\lambda_P)$ and the sink $(\overline{\mathbf{V} \cdot \mathbf{F}}^\lambda_P)$ of kinetic energy (refer to equation 7B4 of the previous paper [35]). In the Tropics, the magnitude and the distribution of the source term are almost identical to those of the sink term. In other words, this figure shows that the kinetic energy produced in the Tropics is mostly

dissipated in the Tropics. Since the scale of tropical eddies is relatively small, the lifetime of these eddies is shorter than of those of the middle latitudes. This may be why the tropical eddies dissipate before the energy is transported elsewhere. It is rather doubtful that such a tropical maximum of eddy kinetic energy does exist in the actual atmosphere. According to our speculation, the simplified scheme of convection adopted for the present study may tend to create too much eddy available potential energy of resolvable scale because of the shortcoming of the criterion for the onset of convection, whereas in the actual atmosphere the heat released by condensation creates cumulus-scale convection and the kinetic energy of the eddies of this scale quickly dissipates instead of producing larger-scale eddies and only occasionally large-scale eddies such as hurricanes may be produced. Further study of tropical convection and the actual distribution of eddies in the Tropics is desirable before it will be possible to engage in a thorough discussion of this subject.

10. MOISTURE BALANCE

A. HEMISPHERIC MOISTURE BALANCE

As table 10A shows, the hemispheric means of the rates of precipitation and evaporation are about 1 m./yr. and coincide very well with the estimate of actual rainfall obtained by Meinardus [20] and Budyko [5, 6].

In our model, the temperature of the earth's surface is determined by the condition of thermal equilibrium at the earth's surface. Therefore, the rate of evaporation and accordingly that of precipitation depend very much upon the radiative energy reaching the earth's surface. The successful simulation of the hemispheric mean rate of rainfall is the natural consequence of the successful simulation of the heat regime at the earth's surface which is discussed in section 11.

B. LATITUDINAL DISTRIBUTION OF MOISTURE BALANCE

In figure 10B1, the latitudinal distributions of precipitation and evaporation for our model atmosphere are compared with those for the actual atmosphere estimated by Budyko [5]. In the model atmosphere, the rainfall exceeds evaporation in the Tropics and in the middle latitudes, and the latter exceeds the former in the subtropics. These features are in excellent qualitative agreement with the observed features of the tropical rain belt, the subtropical desert area, and the rainy region of the middle latitudes. Quantitatively, these results are much more exaggerated in the model atmosphere than in the actual atmosphere. Particularly, the amount of rainfall in the Tropics far exceeds the annual mean of the observed,

TABLE 10A.—*Hemispheric water balance (from 148th day to 187th day)*

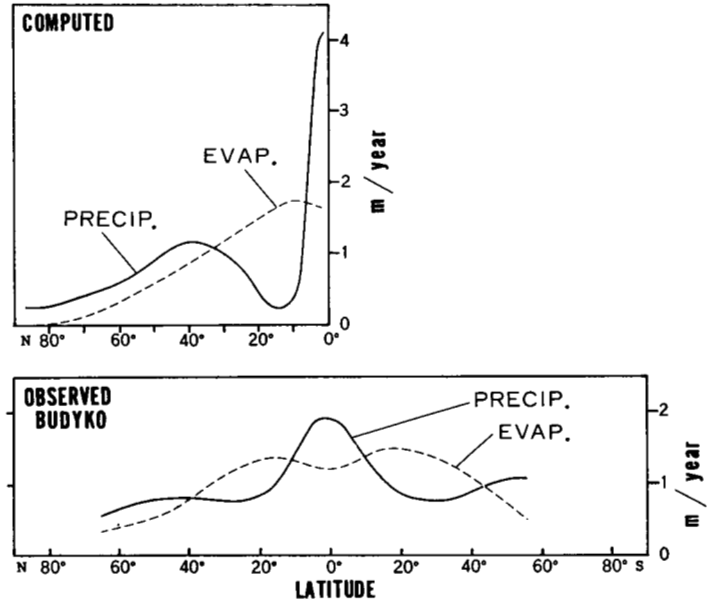|	
Rate of evaporation	105.9 cm./yr.
Rate of precipitation	105.4 cm./yr.
Rate of change of water vapor	−.6 cm./yr.

FIGURE 10B1.—In the upper part of the figure, the latitudinal distributions of precipitation and evaporation obtained from the model are shown, and in the lower part of the figure, observed distributions estimated by Budyko [5] are shown.

and the width of the rain belt is very narrow. Also, the subtropical dry area is located in too low a latitude.

In order to investigate the latitudinal distribution of water balance, figures 10B2 and 10B3 were made. Figure 10B2 shows the latitudinal distributions of moisture transports due to large-scale eddies, meridional circulations, and horizontal subgrid-scale diffusion. The transports by large-scale eddies obtained by Peixoto [27] for the actual atmosphere are also plotted in the same figure. According to this figure and figure 12B3 the excess water produced by evaporation in the subtropics is exported to the Tropics by the meridional circulation and to the middle latitudes by large-scale eddies in both the model and the actual atmosphere. The magnitude of the southward transport of water vapor due to the tropical meridional circulation cell, however, is much larger than that obtained by Peixoto [27] for the actual atmosphere because the exaggerated subtropical desert and the extremely sharp tropical rain belt, which emerged as a result of our time-integration, require a large transport of water from the subtropics into the Tropics. Figure 10B3 shows the latitudinal distributions of various water balance components.[2] Note again that the extremely large sink of water due to condensation in the Tropics is compensated for by the supply of water from meridional circulation. It is rather difficult to pin down the exact causes for the extremely large rainfall in the Tropics at the present

---

[2] The reason the various components do not always balance at each latitude is that interpolation errors occur in converting data from the Cartesian grid of the model to the various latitude circles.
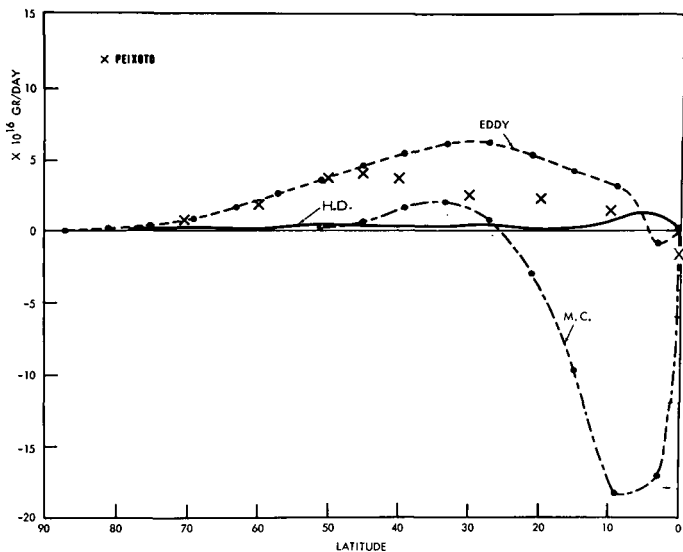
FIGURE 10B2.—The latitudinal distributions of poleward transport of water vapor due to the large-scale eddies (EDDY) the meridional circulation (M.C.), and subgrid-scale diffusion (H.D.). The annual mean of the transport by the large-scale transient eddies in the actual atmosphere obtained by Peixoto [27] is also plotted.
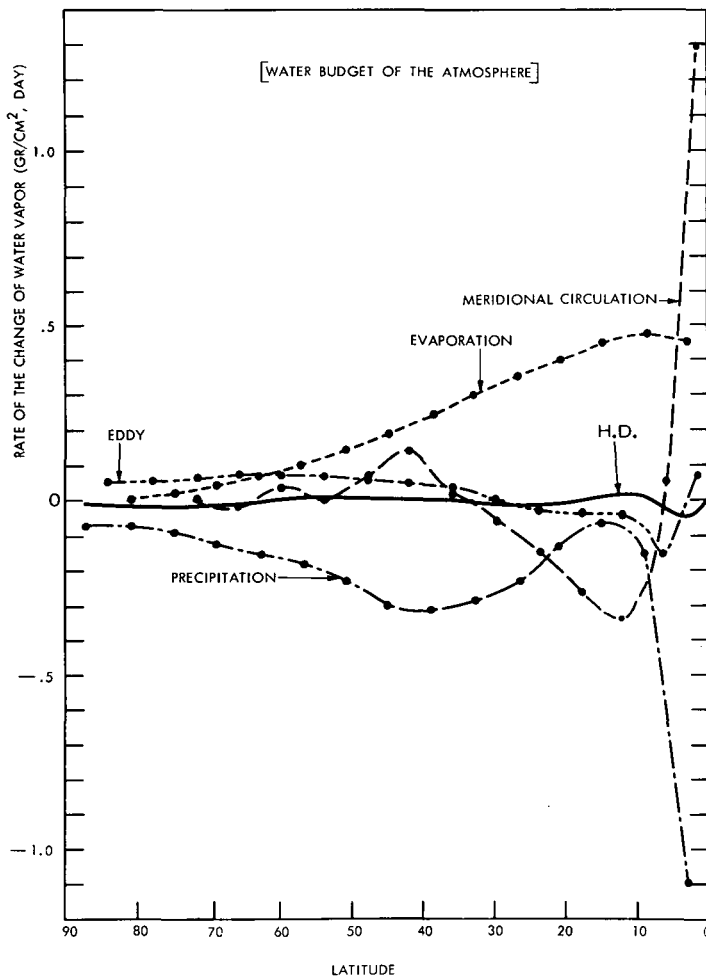

FIGURE 10B3.—The latitudinal distributions of the rate of change of precipitable water due to evaporation, precipitation, large-scale eddies (EDDY), meridional circulation, and horizontal mixing by subgrid-scale turbulence (H.D.).

stage of our investigation. We shall, however, list some of the possible causes:

(1) It is well known that the latitude of the tropical rain belt varies with season. As a result of this variation, the observed maximum of the annual mean rainfall could be less pronounced than the maximum obtained from our model without seasonal variation.

(2) As we explained in the previous paper, the distribution of the vertical mixing coefficient influences the eccentricity of the meridional circulation cell and accordingly the efficiency of the moisture transport due to meridional circulation. The thinner the planetary boundary layer is, the more efficient is the transport. The neglect of vertical mixing of momentum due to moist convection could exaggerate the eccentricity and increase the supply of water vapor into the Tropics.

(3) The existence of the free-slip, insulated equatorial wall of our model fixes the latitude of maximum condensation and causes a concentration of rainfall next to this wall. It is desirable to perform the simulation of the seasonal variation by using a model without an equatorial wall and then to compare the amount of rainfall with the observed annual rainfall.

(4) As figure 12B3 shows, ocean currents transport heat away from the tropical region (refer to sec. 12). Since this process is missing in the present model, excessive evaporation and accordingly excessive rainfall may occur in the tropics of the model atmosphere.

C. LATITUDE-HEIGHT DISTRIBUTION OF MOISTURE BALANCE

In figure 10C1 the latitude-height distribution of the northward transport of water vapor by large-scale eddies and that by both the meridional circulation and large-scale eddies are compared with the corresponding distributions obtained by Peixoto [27] for the actual atmosphere. In both the model atmosphere and the actual atmosphere most of the moisture transport is accomplished in the lowest 300-mb. layer of the atmosphere and the export of water vapor from the subtropics into the Tropics has a sharp maximum very near the earth's surface. This sharp maximum is caused mainly by the meridional circulation and is much more pronounced in our results than in Peixoto's results for the actual atmosphere. The eddy flux of water vapor is mostly positive in the troposphere but is negative in the stratosphere where the mixing ratio of water vapor increases with increasing latitude.

The latitude-height distributions of the vertical transport of water vapor by large-scale eddies, by the meridional circulation, and by both of these processes are shown in figure 10C2. One interesting feature of our results is that the upward flux of water vapor due to large-scale eddies has two maxima—in the Tropics and in the subtropics. The tropical maximum is caused by large-scale eddies created by the release of potential energy in the Tropics. As we discussed in section 9, it is highly questionable that such large-scale eddies predominate in
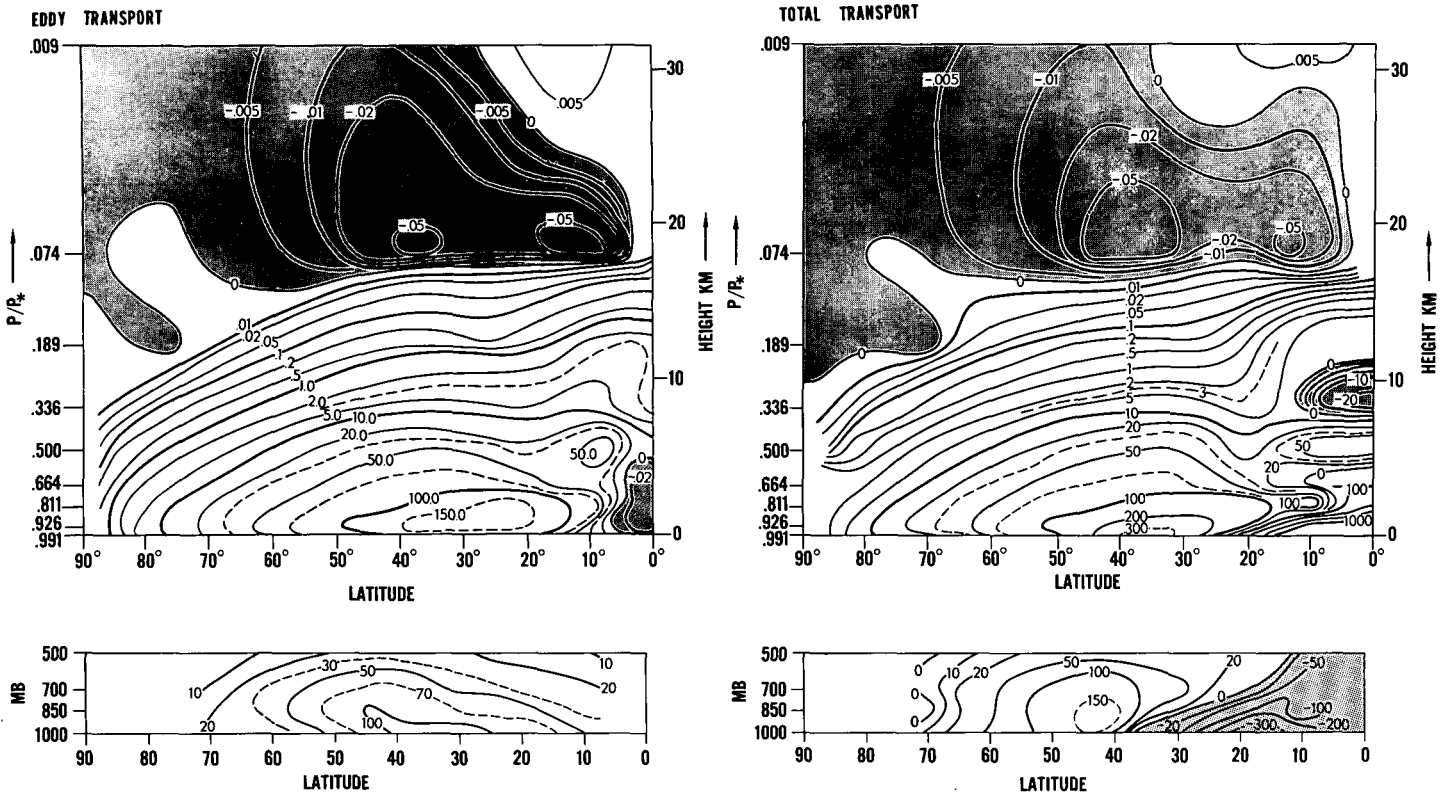
FIGURE 10C1.—Upper part of the figure shows the latitude-height distributions of northward transport of water vapor by the large-scale eddies and that by both the large-scale eddies and the meridional circulation for the atmosphere. Lower part of the figure shows the corresponding distributions for the actual atmosphere obtained by Peixoto [27]. Unit is 10^{12} gm. mb.$^{-1}$ day^{-1}.

the actual tropical atmosphere. Therefore, it may be desirable to improve the scheme of simulating moist convection in order to eliminate the excessive production of large-scale eddies in the Tropics. In order to evaluate the relative importance of the meridional circulation and the large-scale eddies in transporting the moisture upward, figure 10C3 was made to show the hemispheric mean of the vertical transports by these processes of the model atmosphere. From this figure, it is clear that the meridional circulation is much less important than large-scale eddies in transporting moisture upward. The same is true for heat transport, though the meridional circulation transports heat downward as figure 5C2 of the previous paper [35] shows.

The effects of large-scale motion described so far and those of horizontal diffusion compensate for the net change of water vapor caused by evaporation, condensation, and convection as shown in figure 10C4. According to this figure, the source region and sink region of water vapor due to these effects are located in the lower and the upper parts of the model troposphere, respectively. They must be compensated mainly by the effect of large-scale eddies as shown at the bottom of figure 10C2 and in figure 10C3. Note the sink region of water at the level of the tropical tropopause where the temperature is very low and relative humidity is high. As one would expect, there are no

source or sink regions in the rest of the stratosphere because of the lack of moist convection.

D. MOISTURE BALANCE OF THE STRATOSPHERE

According to figure 10C3, the water vapor is transported from the troposphere into the stratosphere mainly by the effect of large-scale eddies. As figure 10C2 shows, the water vapor which is supplied from the troposphere is transported toward low latitudes by both the large-scale eddies and subgrid-scale mixing overshadowing the counteracting effect of the meridional circulation in the low latitudes. The water vapor condenses near the tropical tropopause where the temperature is low and the humidity is high. This condensation is the reason the relative humidity is so low in the rest of the stratosphere of our model. Figure 10D is a schematic representation of eddy transport of water vapor in the stratosphere. In short, the large-scale eddies play a dominant role in transporting the water vapor into the model stratosphere. Our result is quite different from the meridional circulation model proposed by Dobson [8] and that proposed by Brewer [2] for explaining the distribution of various substances in the stratosphere.

At the 34-mb. level ($k=1.5$), the downward transport of water vapor by the large-scale eddies predominates, and the mixing ratio of water vapor at the 9-mb. level
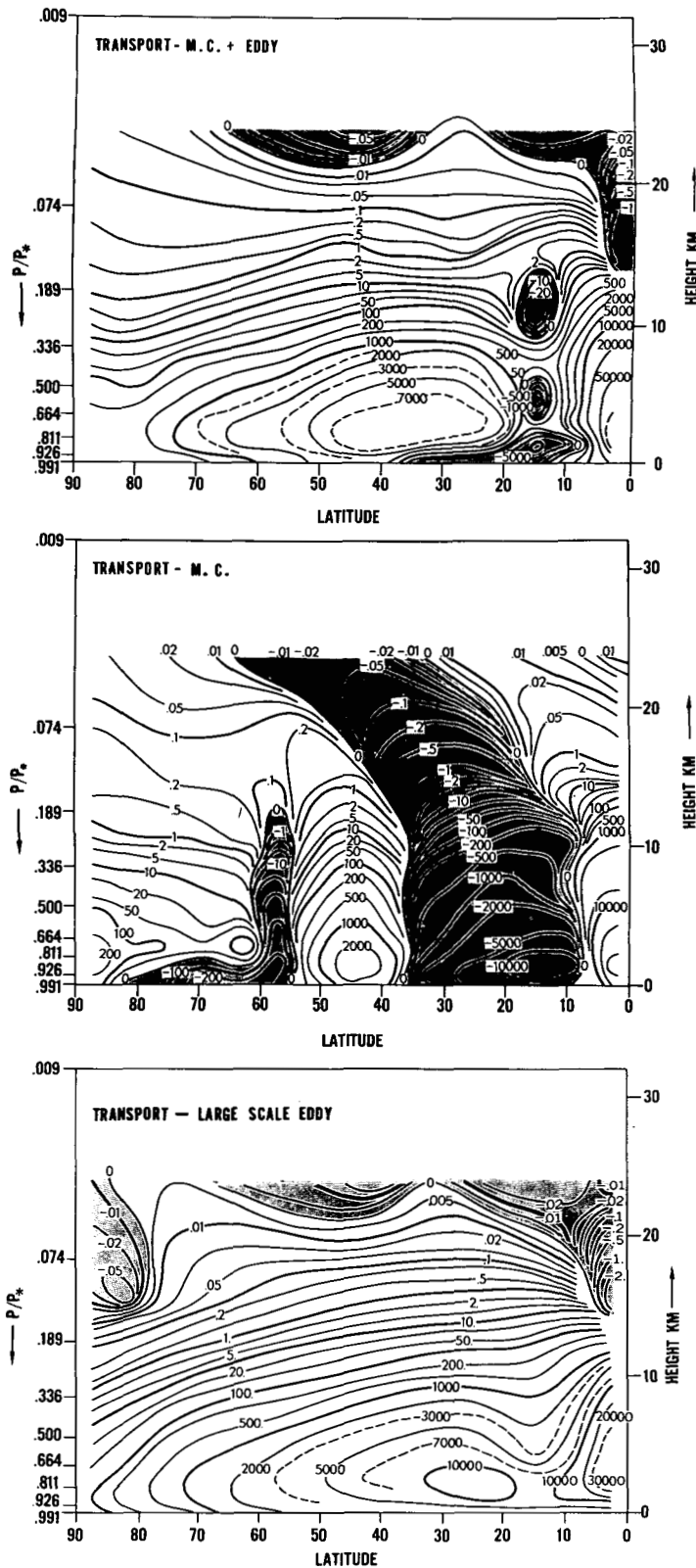
FIGURE 10C2.—The latitude-height distributions of the vertical transport of water vapor by the large-scale eddies, by the meridional circulation, and by both of these two effects are shown in the lower, middle, and upper part of the figure, respectively. Units are 10^{-5} gm. cm.$^{-2}$ day^{-1}.
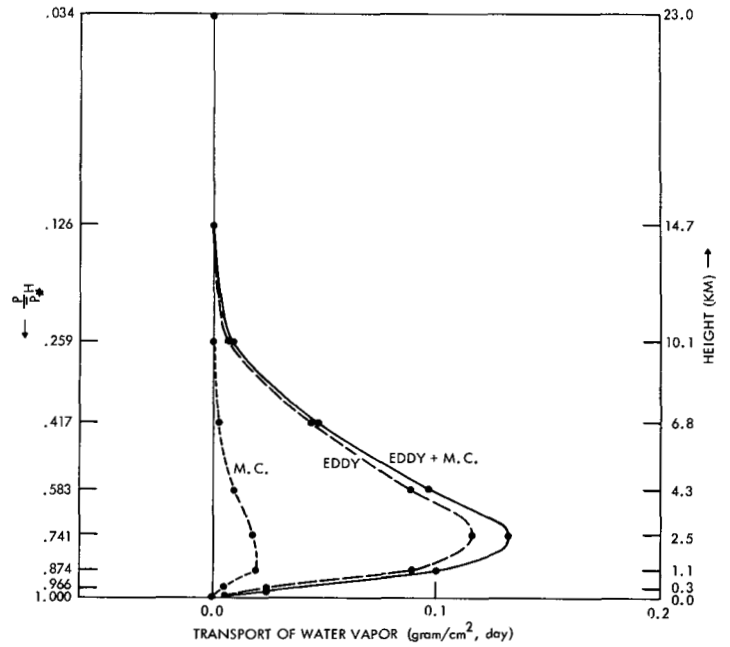
FIGURE 10C3.—Vertical distributions of the hemispheric mean of vertical transport of water vapor by the meridional circulation (M.C.), by the large-scale eddies (EDDY), and by both of these two effects (EDDY + M.C.).
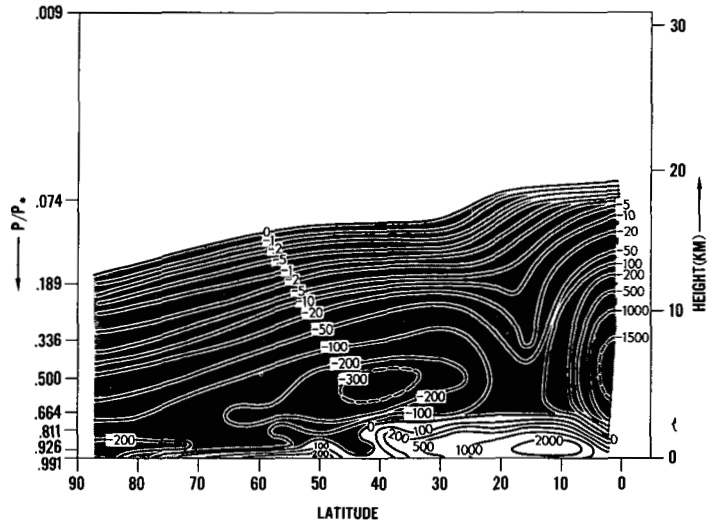
FIGURE 10C4.—Latitude-height distribution of net source of water vapor due to evaporation, condensation, and convection. Units are 10^{-6} (gm. of water vapor/gm. of air)/day.

($k=1$) is significantly smaller than that at the 74-mb. level ($k=2$). It is not clear whether this counter-gradient transport is due to the truncation error of the interpolation of the mixing ratio, which is performed to compute the vertical transport of water vapor, or to the genuine development of an inverse correlation between the absolute humidity and vertical motion. A further increase of vertical resolution is necessary before we can obtain a convincing result.
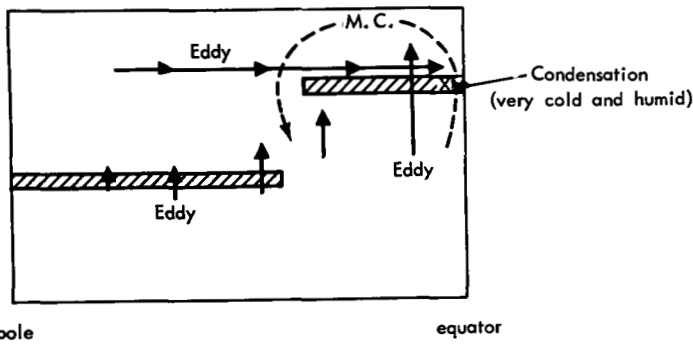
WATER BUDGET OF THE STRATOSPHERE

FIGURE 10D.—Schematic representation of water vapor transport in the stratosphere.
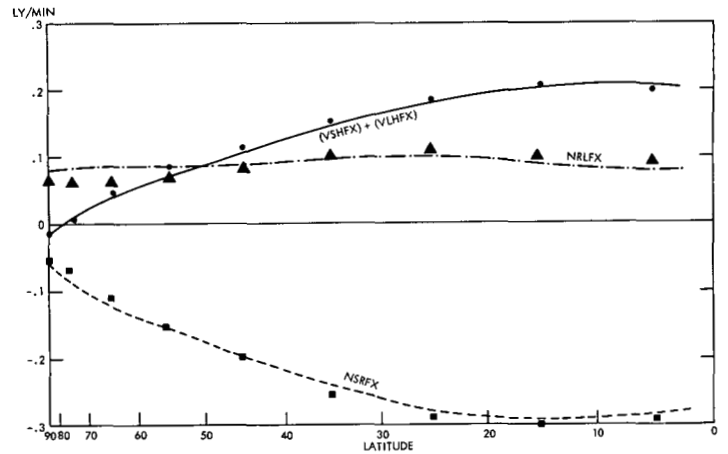

FIGURE 11.1.—Latitudinal distributions of net upward solar radiation (NSRFX), of net upward long-wave radiation (NRLFX), and of upward flux of both latent and sensible heat due to turbulent eddies ((VSHFX) + (VLHFX)). The corresponding distributions obtained by London [17] for the actual atmosphere are also plotted.

11. ENERGY BUDGET OF THE EARTH'S SURFACE

Figure 11.1 shows the latitudinal distributions of various heat balance components at the earth's surface, i.e., the net upward solar radiation, the net upward long-wave radiation, and the sum of the turbulent eddy flux of sensible heat and of latent heat. The corresponding quantities obtained by London [17] for the actual atmosphere are plotted in the same figure. According to our comparison, the coincidence between them is excellent.

In figure 11.2 the latitudinal distributions of both sensible and latent heat flux from the earth's surface are compared with those obtained by Budyko [5] for land, sea, and the whole earth. According to this comparison, our results lie between his results for sea and for the whole earth. Since the relative humidity of the air over oceans which coexist with continents should be smaller than that of the air over the completely wet earth used for our model, these results are reasonable. Using the results given in figure 11.2, the latitudinal distribution of Bowen's ratio, i.e., the ratio of sensible heat flux to latent heat flux at the surface, was computed and is shown in figure 11.3. The distribution of Bowen's ratio for very high latitudes is not computed because the latent energy flux, which is the denominator, tends to zero, and the sensible heat flux, which is the numerator, changes its sign in very high latitudes. In the same figure, Bowen's ratios obtained by Budyko [5] and Jacobs [11] for the ocean are added for comparison. The agreement between the distribution of Bowen's ratio of the model atmosphere with a wet surface and that obtained for the actual ocean is satisfactory.

In short, the energy budget of the earth's surface of our model is very similar to the actual budget obtained by London [17] and the partition of the turbulent energy transport into latent energy flux and sensible heat flux is reasonably close to the partition taking place at the actual ocean surface because of the assumption of the wet surface adopted for our model.
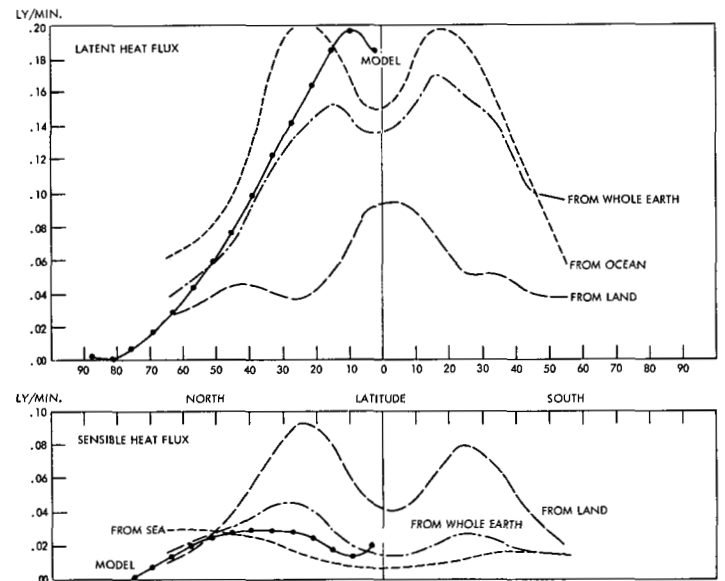

FIGURE 11.2.—Latitudinal distributions of latent and sensible heat flux from the earth to the atmosphere. The distributions, which were obtained by Budyko [5] for land, sea, and the whole earth, are compared with the distributions obtained from our model.
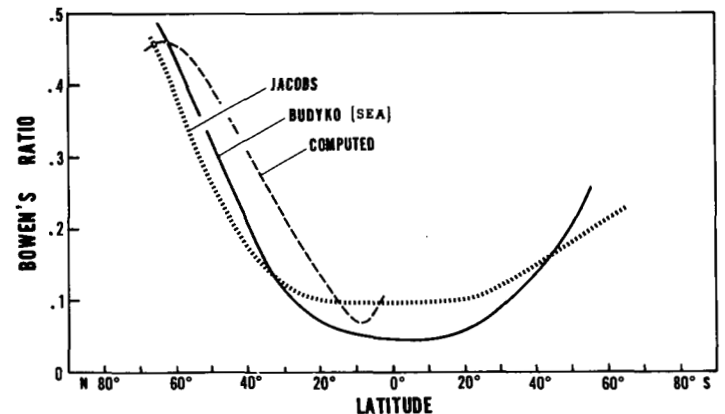

FIGURE 11.3.—Latitudinal distributions of Bowen's ratio obtained by Budyko [5] and Jacobs [11] are compared with that obtained from our present results.

12. HEAT BALANCE

A. HEMISPHERIC HEAT BALANCE

Figure 12A shows the hemispheric mean of heat balance of our model atmosphere and that of the actual atmosphere obtained by London [17] and Budyko [5]. The agreement between the two results is excellent.

B. LATITUDINAL DISTRIBUTION OF HEAT BALANCE

In figure 12B1 the latitudinal distribution of the radiative fluxes at the top of the model atmosphere are compared with those obtained by London [17] for the actual atmosphere. The agreement between them is excellent. The meridional transports of energy expected from the radiative imbalance for both dry and moist general circulation models are given in figure 12B2. The corresponding transports, which were obtained from the results of Houghton [9] and London [17], are also plotted in the same figure. The transport obtained from the moist general circulation model is closer to the observed transport than that from the dry model because of the improvement in the latitudinal gradient of temperature described in section 5.

In the actual earth-atmosphere system, the meridional transport of energy required from radiative imbalance must be accomplished by the following three processes:

(1) Northward transport of total energy $(=c_p T + \phi + K)$ in the atmosphere. ϕ is geopotential, and K is total kinetic energy per unit mass.

(2) Northward transport of latent energy in the atmosphere.

(3) Northward transport of total energy in the oceans.

Figure 12B3 shows the latitudinal distributions of these three transports which are calculated by use of the results of Houghton [9] and Budyko [5], [6].[3] The transport of

---

[3] The latitudinal distribution of rainfall is obtained from Budyko [6].

latent energy (2) is obtained by integrating the difference between evaporation and precipitation with respect to latitude. The transport of energy by the oceans (3) is computed by integrating the thermal imbalance at the earth's surface. A similar computation was performed by Bryan [3]. In order to perform these integrations, Budyko's data for the Northern Hemisphere and the Southern Hemisphere are averaged. The meridional transport of total energy in the atmosphere (1) is calculated as the difference between the transport expected from radiative imbalance and the net transport due to the two other effects (2, 3). The northward transport of latent energy which is computed by Peixoto [27] for the Northern

FIGURE 12B1.—Latitudinal distribution of net downward solar radiation (SR) and of net upward long-wave radiation (LWR) at the top of the atmosphere.
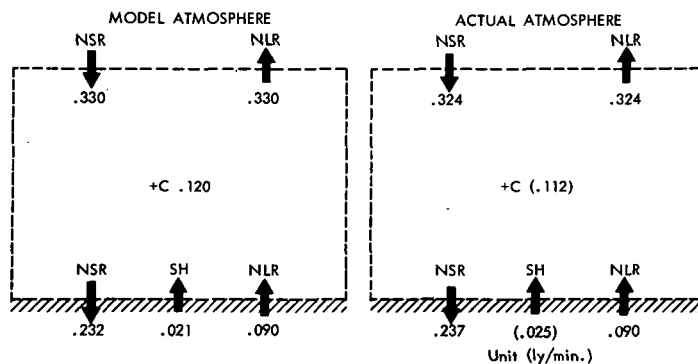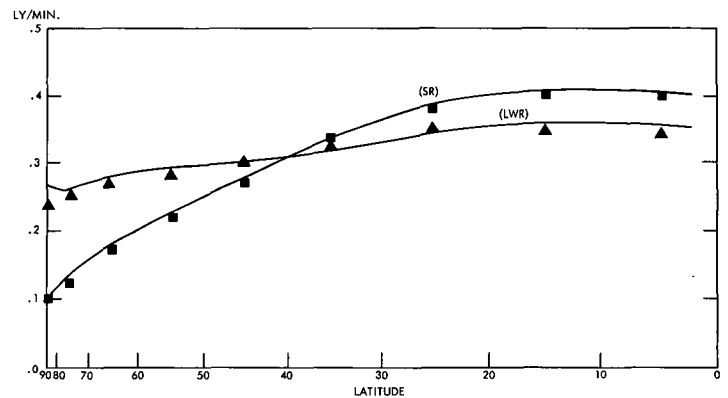
FIGURE 12A.—Hemispheric mean of the heat balance of the model (left) and actual atmosphere (right). The heat balance components of actual atmosphere are obtained by London [17] and Budyko [5, 6]. NLR=net long-wave radiation [17]. NSR=net solar radiation [17]. SH=sensible heat flux [5]. C=heat of condensation [5].
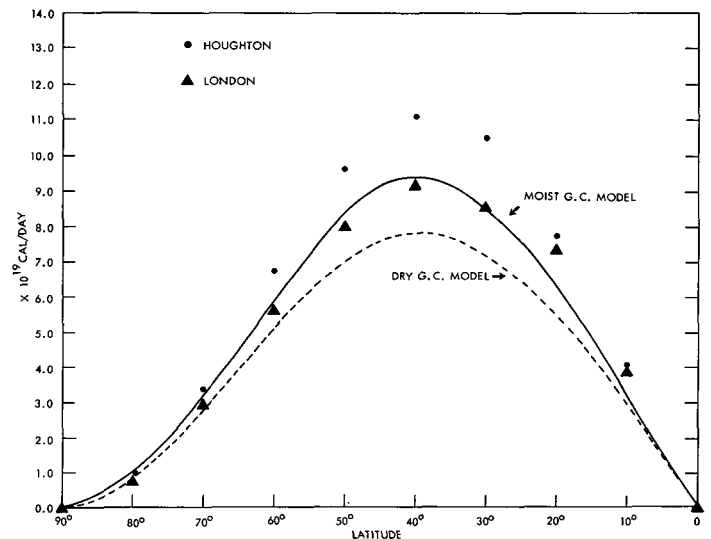
FIGURE 12B2.—Latitudinal distributions of meridional transport of energy expected from the radiative imbalance of the earth-atmosphere system. The results obtained from both dry and moist general circulation models are compared with the corresponding distributions obtained by Houghton [9] and London [17] for the actual situation.

Hemisphere is plotted in the same figure and agrees well with the corresponding flux estimated above.

In figure 12B4 the latitudinal distribution of the meridional transport of total energy $(c_pT+\phi+K)$ and that of latent energy in the model atmosphere are shown. The energy transport in the ocean is missing because of the assumption of a wet land surface on the earth. According to this figure, in both the actual and model atmosphere, an equatorward transport of latent energy by the meridional circulation predominates in the low latitudes and a poleward transport by the large-scale eddies predominates in middle latitudes. The magnitude of these transports in the model atmosphere, however, is larger than in the actual atmosphere. In order to compensate for the large southward transport of latent heat, an extremely large poleward transport of total energy appears in low latitudes. Both of these transports are accomplished by the intense meridional circulation which predominates in the low latitudes of our model atmosphere. Because the northward transport of latent energy is by large-scale eddies in middle latitudes, the meridional transport of total energy $(c_pT+\phi+K)$ in middle latitudes is significantly smaller than the net energy transport expected from radiative imbalance. In the dry model the meridional transport of total energy in the atmosphere, however, is identical with the net transport which is expected from radiative imbalance and is shown in figure 12B2. Figure

12B5 shows the comparison between the meridional transport of sensible heat by large-scale eddies in the moist atmosphere and in the dry atmosphere. The former is significantly smaller than the latter and is closer to the transport obtained by Starr and White [38] for the actual atmosphere. This is why the temperature gradient in the middle latitudes obtained from the present model is somewhat smaller than that obtained from the dry general circulation model. For comparison, the latitudinal distribution of the transport of latent energy is shown in the lower half of figure 12B5.

In figure 12B6 the latitudinal distributions of the net thermal imbalance of the earth-atmosphere system of the model due to radiative transfer and condensation are compared with the corresponding imbalance in the actual atmosphere estimated by use of the results of Budyko [5], [6] and Houghton [9]. One of the characteristic features of the present result is the large excess of heating in the Tropics and the large deficit in the subtropics. Although this feature agrees qualitatively with observation, the magnitude of the excess and the deficit are much larger than those of the actual atmosphere. This thermal
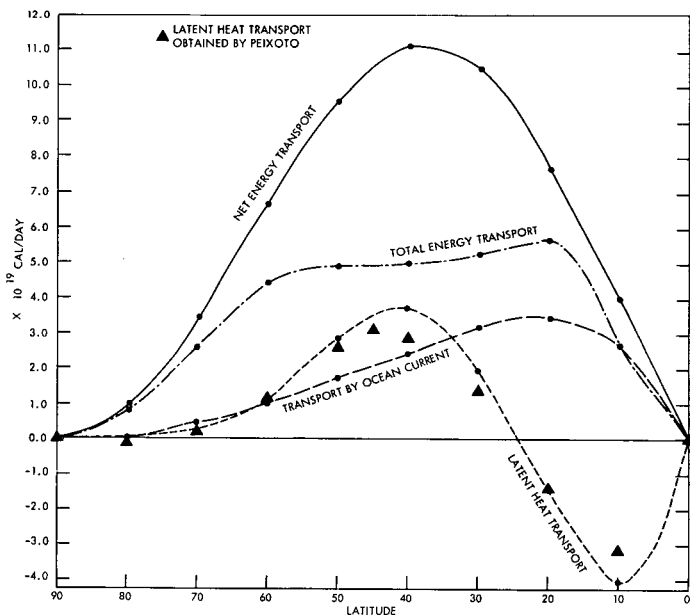

Figure 12B3.—The latitudinal distribution of poleward net energy transport of the earth-atmosphere system, which is expected from the radiative imbalance, is shown together with the transport of total energy $(c_pT+\phi+K)$ and that of latent energy in the atmosphere, and the transport of energy by ocean currents. The estimate of these transports was made by use of the data obtained by Budyko [5], [6] (average of values for both hemispheres) and Houghton [9]. The meridional transport of latent energy obtained by Peixoto [27] is plotted for comparison.
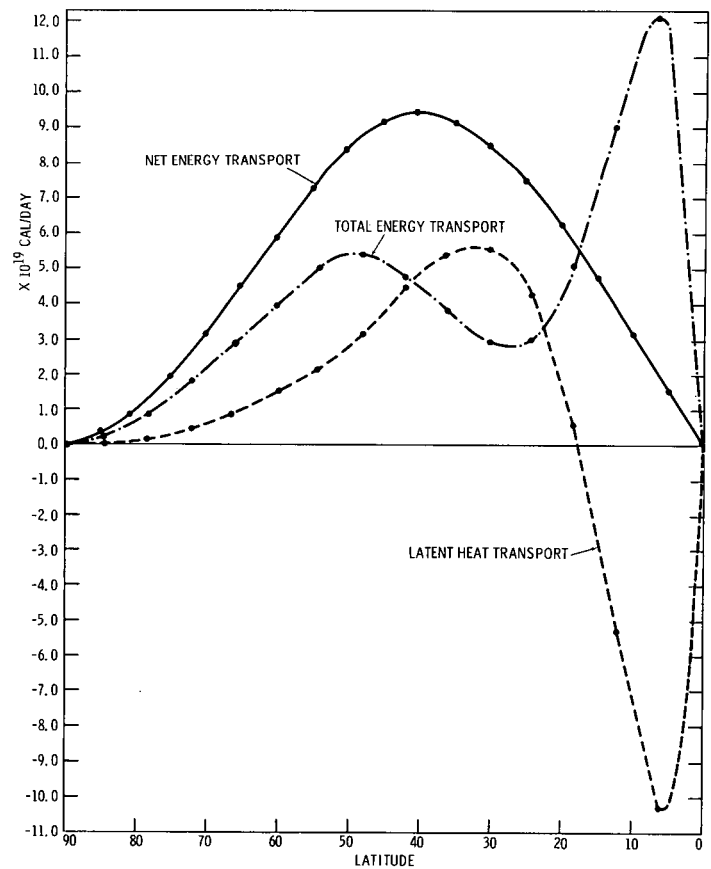

Figure 12B4.—The net energy transport expected from the radiative imbalance and the transport of total energy $(c_pT+\phi+K)$ and latent energy in the model atmosphere. The flux of latent energy is computed by integrating the latitudinal distribution of the imbalance of water.
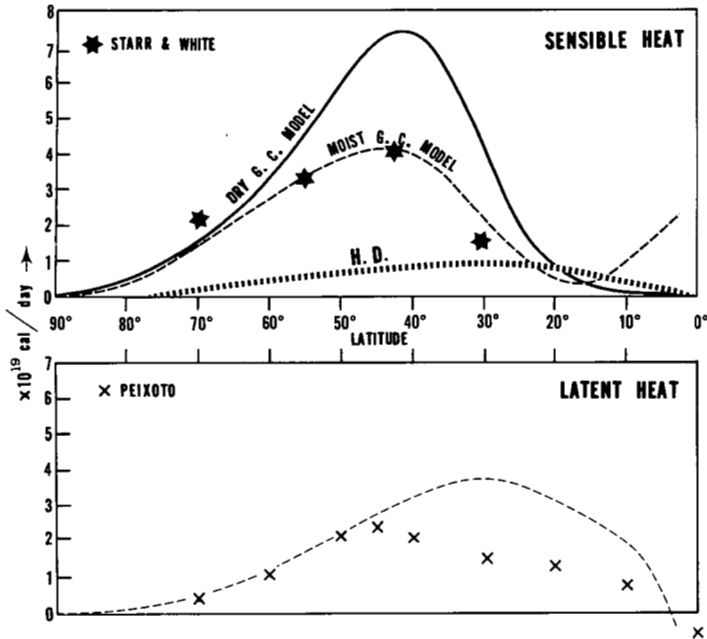
FIGURE 12B5.—In the upper part of the figure, the latitudinal distributions of the meridional transport of sensible heat by large-scale eddies, which are obtained from both dry and moist general circulation models, are shown together with that resulting from the subgrid-scale mixing (H.D.). Also, that of the sensible heat flux obtained by Starr and White [38] for the actual atmosphere is plotted for comparison. In the lower part of the figure, the meridional transport of latent energy in the model atmosphere is compared with the corresponding distribution obtained by Peixoto [27] for the actual atmosphere.
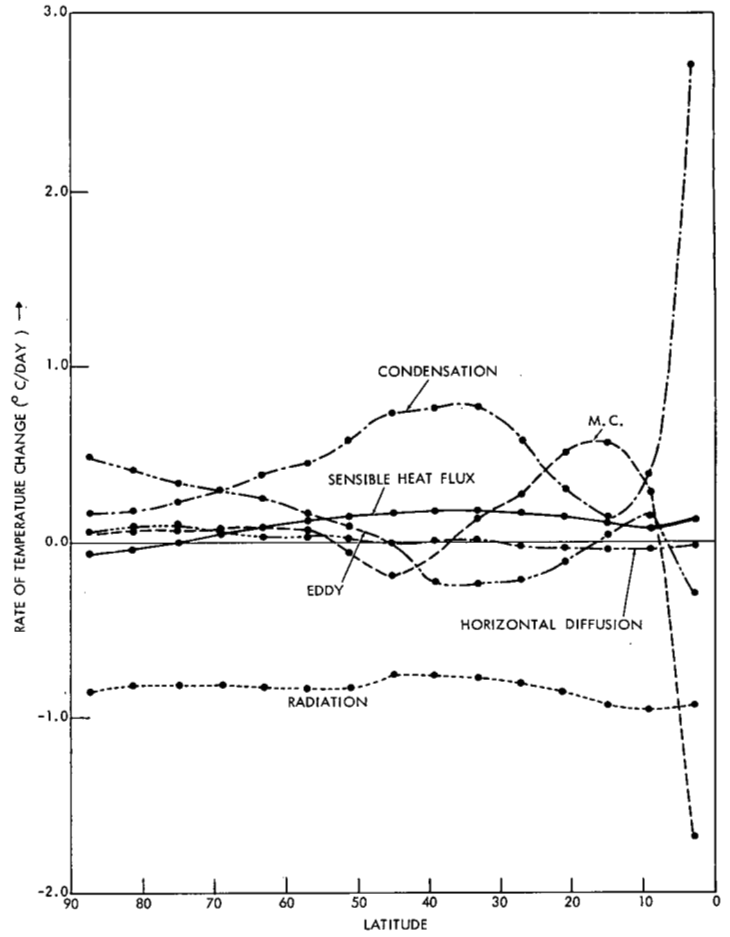

FIGURE 12B7.—The latitudinal distributions of the rate of temperature change in the model atmosphere by condensation, radiation, sensible heat flux from the earth's surface, the meridional circulation (M.C.), the large-scale eddies (EDDY), and horizontal subgrid-scale mixing (HORIZONTAL DIFFUSION).
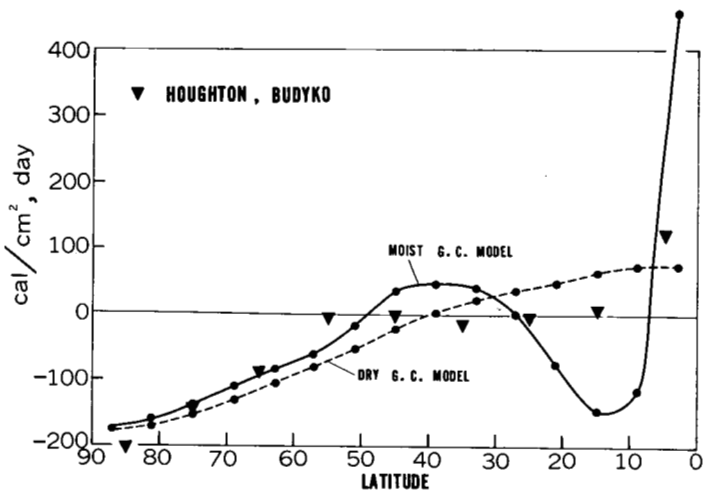

FIGURE 12B6.—The latitudinal distributions of the net thermal imbalance caused by the effect of condensation and radiation, and the transport of sensible heat from the earth's surface. Solid and dashed lines show the results of the moist and dry general circulation models, respectively. The corresponding distribution for the actual atmosphere, which is computed from the results of Budyko [5], [6] and Houghton [9], is shown by triangles.

imbalance must be compensated for by the effect of large-scale motion. Figure 12B7 shows the latitudinal distribution of all the heat balance components obtained from the present results. According to this figure, the large amount of heat released by condensation in the Tropics is mainly compensated for by the cooling caused by the meridional circulation. In the subtropics the radiative cooling is compensated for by the sensible heat flux from the earth's surface and the heating caused by the downward branch of the meridional circulation; in middle latitudes the radiative cooling is mainly counteracted by the heat of condensation; and in high latitudes it is compensated for by the heating caused by the convergence of heat transport from large-scale eddies and heat released by condensation.

C. LATITUDE-HEIGHT DISTRIBUTION OF HEAT BALANCE

The lower part of figure 12C1 shows the latitude-height distribution of the rate of temperature change caused by convection and condensation obtained from the integration of the moist general circulation model. For com-
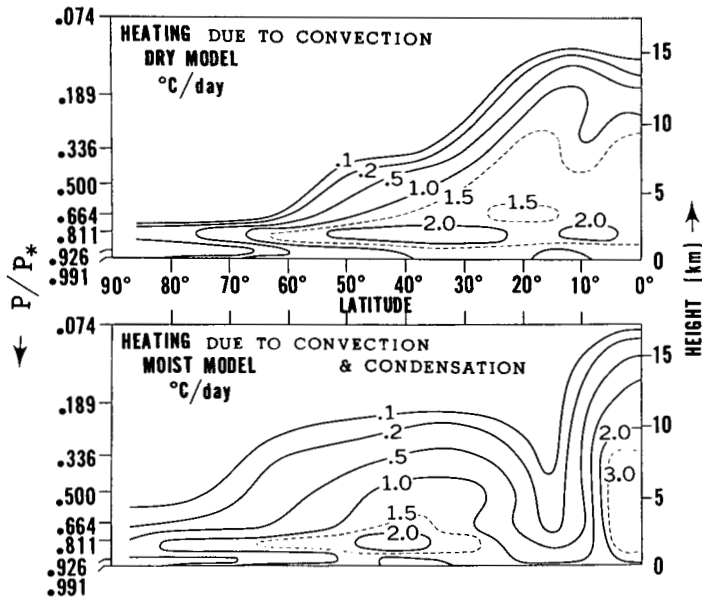
FIGURE 12C1.—In the upper part of the figure the latitude-height distribution of the rate of the net temperature change in °C./day caused by the sensible heat from the earth's surface and the moist convective adjustment in the dry general circulation model. In the lower part, that caused by the heat of condensation, the sensible heat flux from the earth's surface, and the vertical heat flux due to convection is shown for the moist model.
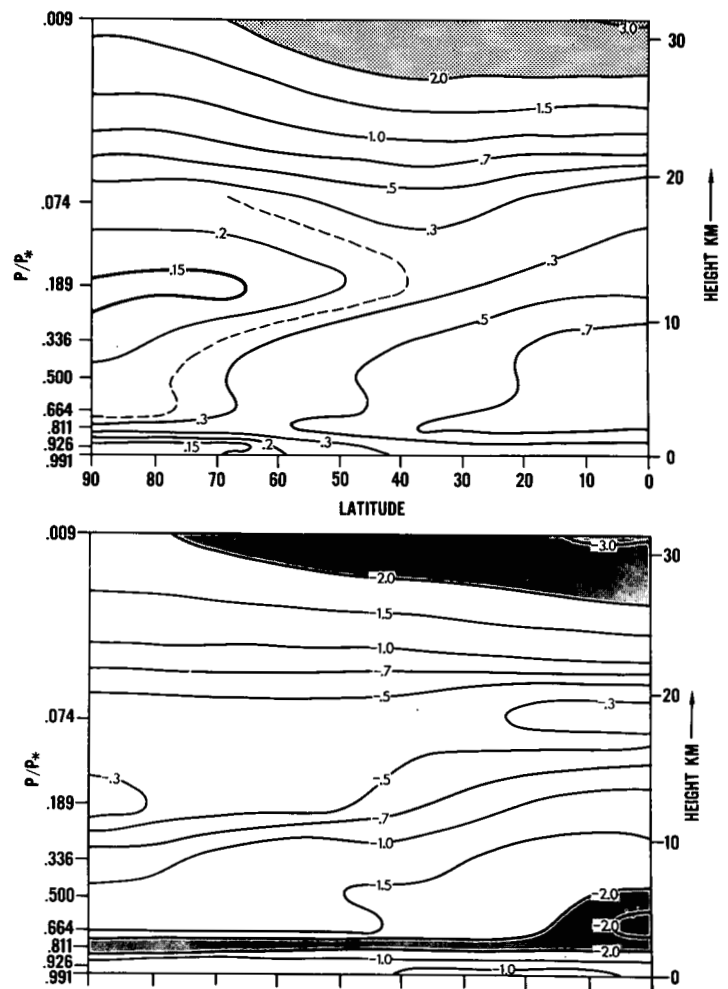

FIGURE 12C2.—The latitude-height distribution of the rate of temperature change in °C./day due to solar radiation and that due to long-wave radiation are shown in the upper and lower part of the figure, respectively.

parison the latitude-height distribution of the rate of temperature change due to moist convective adjustment and vertical mixing obtained from integration of the dry model is shown in the upper part of this figure. The former has two pronounced maxima; one is located in the Tropics, and the other in middle latitudes. On the other hand, the latter has only one maximum near the Tropics and the intensity of heating decreases monotonically with increasing latitude. The height of the tropical convective tower of the moist model atmosphere is taller than that of the dry model atmosphere. In the sub-tropics, the convective activity of the moist model atmosphere is limited to the layer close to the earth's surface, whereas that of the dry model atmosphere reaches high altitudes. In high latitudes, the temperature change due to the heat of condensation in the moist model atmosphere is larger than that of the dry model atmosphere because of the meridional transport of latent energy from middle latitudes. The general features of the latitude-height distribution of the rate of radiative temperature change for the moist model are very similar to those in the previous results. Figure 12C2 shows the latitude-height distribution of long-wave radiation and of solar radiation. Refer to the previous paper [35] and the paper by Manabe and Strickler [18] for a detailed discussion of the distribution of the radiative temperature change.

The computed distribution of the net rate of temperature change due to radiation, convection, and condensation are compared with a similar distribution obtained

by Albrecht [1] for the actual atmosphere in figure 12C3. Note the net destabilizing effect of the combination of these processes. This destabilizing effect must be compensated for by the meridional circulation and the large-scale eddies. For example, the meridional circulation is the major counteracting factor in the subtropics, and the large-scale eddies have a stabilizing effect in middle latitudes. Figure 12C4 shows the latitude-height distributions of both the northward and upward transport of heat due to large-scale eddies. According to the comparison between this figure and figures 5D3 and 5D4 of the previous paper, the magnitudes of both vertical and horizontal flux in middle latitudes are significantly smaller than those obtained from the dry general circulation model. It is noteworthy that in middle latitudes the baroclinic activity is less for the moist model than for the dry general circulation model. Another feature of interest is the maximum vertical eddy flux of heat in the Tropics which is caused by the heat of condensation. The result-
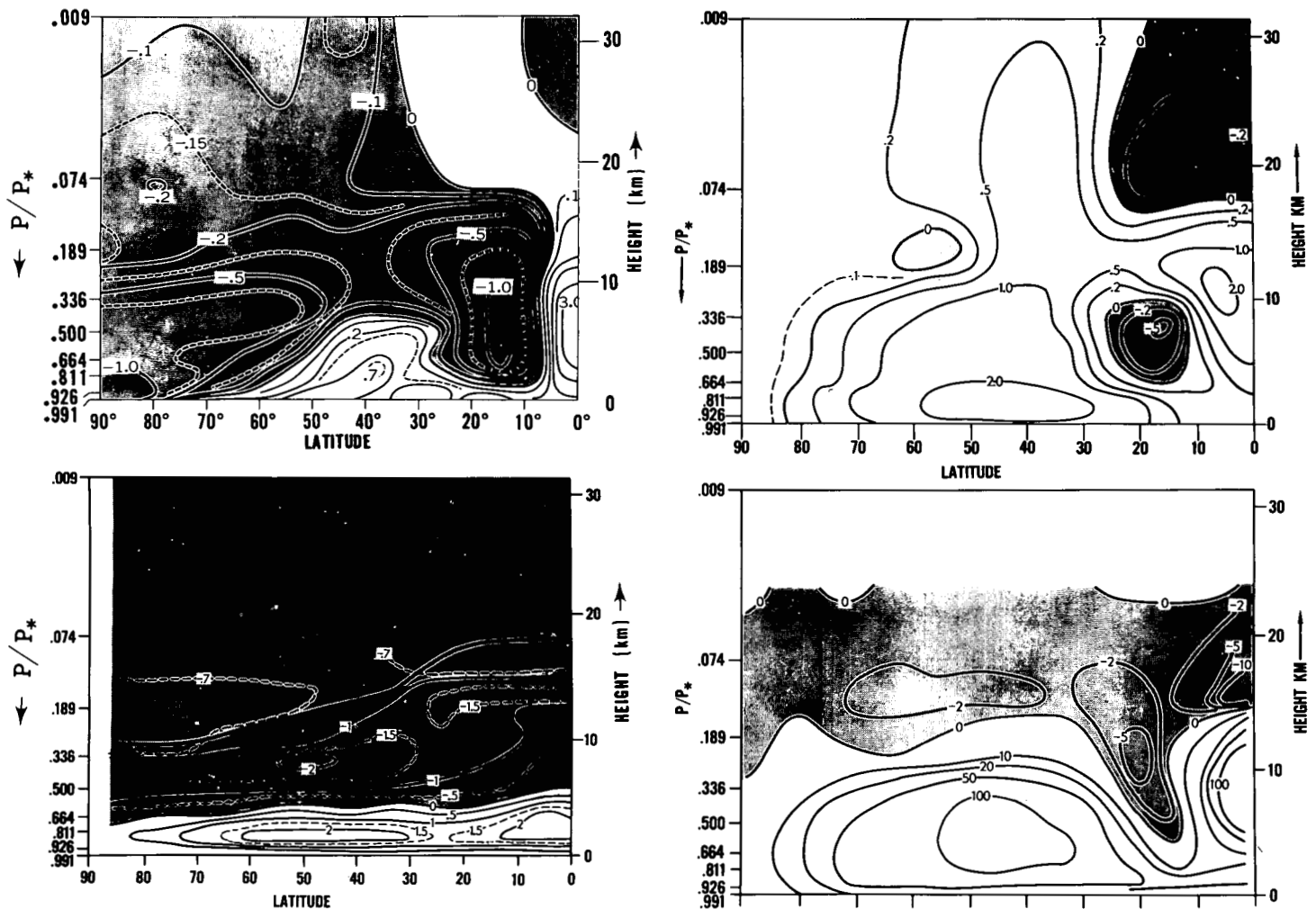
FIGURE 12C3.—The latitude-height distribution of the net rate of the change of temperature in °C./day due to radiation, convection, and condensation for the model atmosphere and the actual atmosphere are shown in the upper and lower part of the figure. The latter is estimated by Albrecht [1]. Heavy line is observed tropopause.

FIGURE 12C4.—Latitude-height distributions of the northward transport of heat (10^{17} joule mb.$^{-1}$ day^{-1}) and that of the upward transport of heat (joule cm.$^{-2}$ day $^{-1}$) by the large-scale eddies are shown in the upper and lower part, respectively.

ant release of potential energy creates a tropical maximum of eddy kinetic energy. Refer to section 9 for a further discussion of this result.

13. ANGULAR MOMENTUM BALANCE

In figure 13.1, the latitudinal distributions of the northward transport of momentum by various processes are shown. One of the characteristic features of this result is the large transport of momentum by the meridional circulation in low latitudes. This result is consistent with the very large transport of water vapor and of heat described in sections 10 and 12.

In figure 13.2, the latitudinal distribution of the transport of angular momentum by large-scale eddies obtained from the present computation is compared with that obtained from our previous computation. The northward transport in the actual atmosphere, as evaluated by Buch [4] and Starr and White [38], is plotted in the same figure.

According to this figure, the actual eddy transport lies between the results of the dry and moist computations. As described in section 12, the heat transport by large-scale eddies is also less for the present result than for the previous result [35]. In short, the heat of condensation decreases the temperature gradient and the vertical wind shear in middle latitudes, decreases the eddy kinetic energy in middle latitudes, and accordingly decreases the northward fluxes of heat and momentum due to large-scale eddies. Recently, we performed an integration of the dry general circulation model with high resolution ($N=40$). As equation (2B8) of the previous paper [35] shows, the coefficient of subgrid-scale diffusion of momentum and heat is proportional to the square of the grid size and to the absolute value of the deformation. According to our results the effective Reynolds number seems to increase with increasing resolution. The transport of heat and momentum by the large-scale eddies as well as
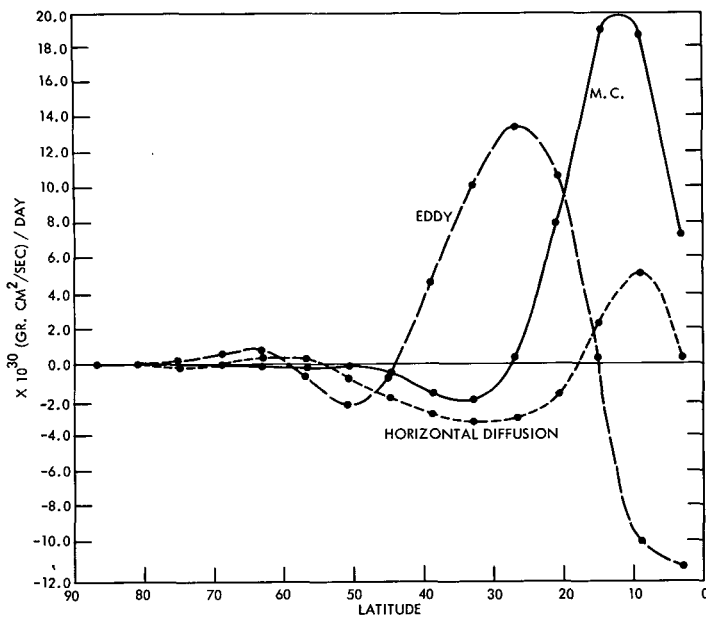
FIGURE 13.1.—Latitudinal distributions of poleward transport of angular momentum by the meridional circulation (M.C.), the large-scale eddies (EDDY), and the horizontal subgrid-scale mixing (HORIZONTAL DIFFUSION).

the magnitude of the eddy kinetic energy are much larger for the (N=40) experiment than for the (N=20) experiment. Smagorinsky and staff members [36] performed a series of forecasting experiments using the present moist general circulation model and concluded that the increase of resolution from (N=20) to (N=40) greatly improved the results, especially in regard to vertical motion and precipitation. It is therefore desirable to perform a numerical general circulation experiment using the moist model with high resolution (N=40).

In figure 13.3, the latitudinal distribution of surface torque obtained from the present integration is compared with that from the previous computation. In the same figure, the values of the stress on the actual earth's surface, which were computed by Priestley [29] for both winter and summer, are plotted as reference. According to this figure, the torque obtained from the present integration is smaller than that of the previous study. Another notable feature in the present result is the systematic shift of the mode of angular momentum exchange between the earth and the atmosphere toward the low latitudes. This result is consistent with the fact that the width of the upward-motion branch of the tropical meridional circulation cell in the model atmosphere is very small.

14. CONCLUDING REMARKS

In a numerical experiment some of the features of the hydrologic cycle in the earth-atmosphere system are simulated successfully. In the tropical troposphere of our model atmosphere the relative humidity is high and rainfall
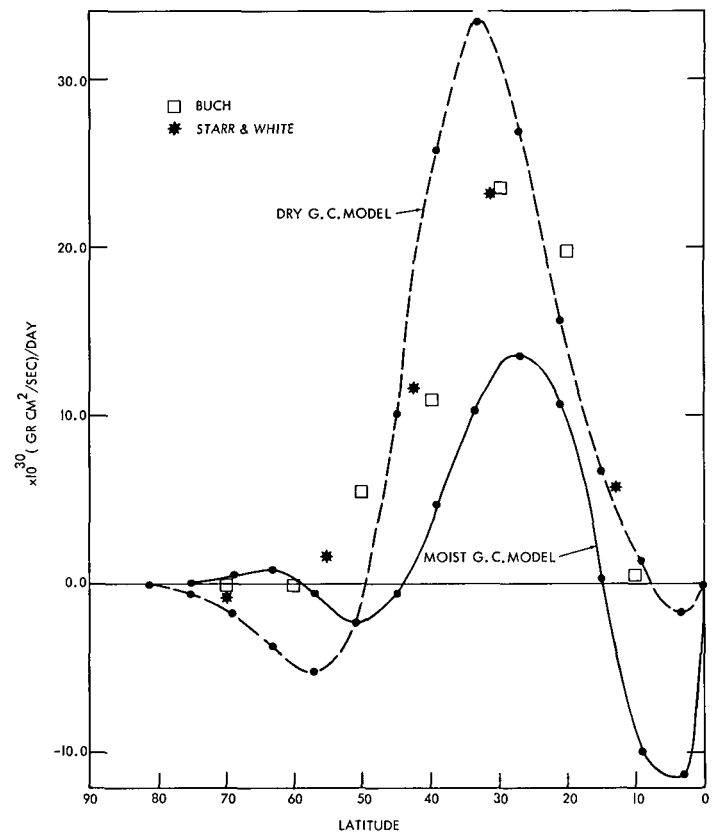

FIGURE 13.2.—Latitudinal distributions of the poleward transport of angular momentum by the large-scale eddies in the moist model atmosphere and the dry model atmosphere. Values obtained by Buch [4] and Starr and White [38] are also plotted.
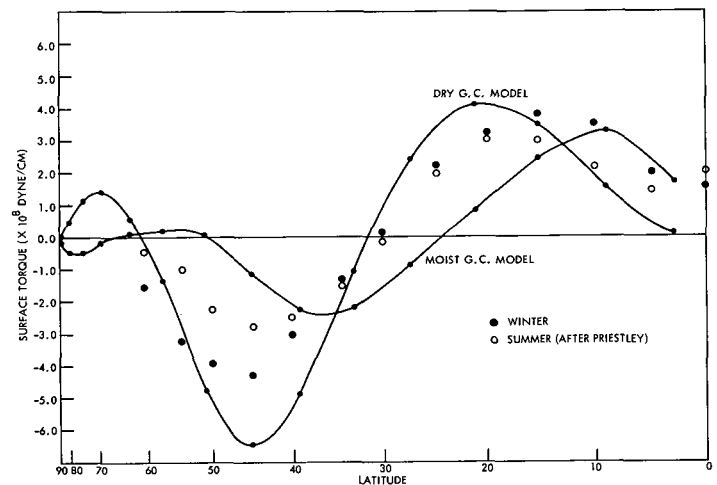

FIGURE 13.3.—The latitudinal distributions of surface torque obtained from dry and moist general circulation models are compared with the estimate by Priestley [29] for both winter and summer situation.

exceeds evaporation; and in the subtropics the relative humidity is low and the evaporation is higher than precipitation. The excess water vapor thus created in the subtropics is exported to the Tropics by the meridional circulation and to middle latitudes by the large-scale eddies. Generally speaking, the relative humidity decreases with increasing altitude. In the stratosphere of our model atmosphere the relative humidity is very low except at the tropical tropopause and the mixing ratio of water vapor is very small in agreement with the actual atmosphere. The hemispheric mean of precipitation obtained from our computation is 1.06 m./yr. and agrees reasonably well with the value of 1 m./yr. estimated by Budyko [5] and Meinardus [20] for the actual atmosphere. At the top of the model atmosphere the latitudinal distribution of the net solar radiation and long-wave radiation coincide very well with those estimated by London [17] for the actual atmosphere. At the earth's surface the latitudinal distribution of the vertical turbulent flux of energy as well as that of the radiative fluxes also agrees with the results of London [17]. Bowen's ratio at the wet earth's surface adopted for the model agrees well with that obtained for the ocean surface by Budyko [5] and Jacobs [11].

Quantitatively, there are many features of the computed hydrologic cycle which disagree with the observed features. Both the rain belt in the Tropics and the dry belt in the subtropics are exaggerated too much. As a result, the southward transport of water vapor by the meridional circulation in the Tropics is extremely large. Generally speaking, the relative humidity of the moist layer at the earth's surface is too large. Therefore, the model atmosphere has a significantly larger amount of precipitable water than the annual mean amount of the actual atmosphere.

Unfortunately, very little is known about the hydrologic cycle in the stratosphere because of the difficulty in performing routine measurements. In our model, water vapor is supplied from the troposphere into the stratosphere mainly by the effect of large-scale eddies. It is then transported toward the tropical tropopause, where the temperature is very low and relative humidity is high, and condenses. Because of this transport and condensation a very dry stratosphere is maintained.

There are many significant differences between the present results and those obtained from the integration of the dry general circulation model:

(1) The intensity of the meridional circulation in the Tropics is larger in the present result than in the previous result because of the effect of moist convection in the Tropics. Also the width of the upward motion branch of the cell is less for the present result. Because of this difference the meridional transport of momentum, heat, and water vapor by the meridional circulation in the Tropics is also very large in the present result. Also, as a consequence of this strong cell we get a very strong subtropical jet stream in the present result.

(2) In the middle latitudes the poleward transport of total energy $(c_p T + \phi + K)$ is significantly smaller for the moist model than for the dry model because of the meridional transport of latent energy in the present model, and the latitudinal temperature gradient in the troposphere of middle latitudes is smaller for the former than for the latter. Therefore, the intensity of the zonal current in middle latitudes obtained from the moist model is smaller and more realistic.

(3) In the stratosphere, the latitudinal increase of temperature obtained from the present study is somewhat larger than that of the previous study. Accordingly, the latitude of the maximum zonal current in the stratosphere increases significantly with increasing altitude in qualitative agreement with the features of the actual atmosphere.

(4) The heat of condensation tends to increase the wave number of the vertical motion significantly. Accordingly, it also increases the wave number of horizontal motion in the troposphere and that of the surface pressure field.

(5) One of the characteristic features of our present result is the tropical maximum of the eddy kinetic energy caused by the release of eddy available potential energy. This available potential energy is created by heat released by convective condensation. Therefore, this tropical maximum of eddy kinetic energy is missing in the results of the dry model. Although this feature seems to be highly unrealistic, further study of convection in the Tropics is desirable before we will be able to determine how unrealistic or realistic this feature is.

(6) The eddy kinetic energy in middle latitudes is significantly smaller for the moist model than for the dry model. Consistent with this difference, the northward transport of momentum and heat due to large-scale eddies is smaller for the former than for the latter.

As we mentioned earlier (sec. 13), the results obtained from the dry model with high resolution ($N=40$) are quite different from those obtained from the dry model with the resolution adopted for the present study ($N=20$). Moreover, the release of heat of condensation tends to decrease the characteristic scale of motion, as we pointed out earlier. Accordingly, the moist model requires higher resolution than the dry model. An examination of the maps of relative humidity and those of vertical velocity suggests that we need higher resolution to properly represent these fields. Therefore, the present result with a relatively coarse resolution may be regarded as a preliminary result before we perform the integration of the model with higher resolution.

Another shortcoming of the model is the existence of a free-slip insulated wall at the equator. This may be part of the reason we get an exaggerated tropical rain belt. It is planned to perform an integration by use of a model without a tropical wall.

As mentioned in the introduction, we computed the rate of the temperature change due to radiation using the climatological distribution of water vapor and clouds instead of the distribution obtained from the prognostic equation of water vapor. In order to study the complete interaction among the radiative transfer, the hydrologic cycle, the photochemistry of ozone, and the large-scale motion, it is necessary to eliminate this constraint and to calculate the radiative transfer based upon the distribution of water vapor and ozone obtained from our model itself.

APPENDIX—NON-CONVECTIVE CONDENSATION (ITERATIVE METHOD)

As an example, we shall describe the iteration method used in computing the non-convective condensation at constant pressure. In our model the relative humidity h is defined as,

$$h = r/r_s \tag{A-1}$$

Linearizing equation (3.3), and replacing δr and δT by Δr and ΔT, respectively, we find the required change in r is approximately:

$$\Delta r = r_s(1-h) + \left(\frac{\partial r_s}{\partial T}\right)_P \Delta T \tag{A-2}$$

where $(\partial r_s/\partial T)_P$ denotes the differentiation of r_s with respect to T at constant pressure. Again replacing δr and δT by Δr and ΔT, equation (3.4) may be written as

$$\Delta T = -\frac{L}{c_p} \Delta r \tag{A-3}$$

Solving (A-2) and (A-3) simultaneously, we get

$$\Delta r = \frac{r_s(1-h)}{1 + \frac{L}{c_p}\left(\frac{\partial r_s}{\partial T}\right)_P} \tag{A-4}$$

The approximate value of $(\partial r_s/\partial T)_P$ is computed by using the definition of r_s and the Clausius-Clapeyron equation

$$\frac{de_s}{dT} = \frac{Le_s}{R^* T^2} \tag{A-5}$$

where R^* is the gas constant for water vapor, and e_s is the saturation vapor pressure.

$(r+\Delta r)$ and $(T+\Delta T)$ are then put into equations (A-1) and (A-4) to obtain higher order increments ΔT and Δr. This cycle is repeated until h is sufficiently close to 1 (100 percent). The process converges very rapidly, usually requiring only one or two steps to bring h within 1 percent of saturation.

The δr and δT of equation (3.3) are.

$$\delta r = \Delta r^1 + \Delta r^2 + \ldots + \Delta r^n$$
$$\delta T = \Delta T^1 + \Delta T^2 + \ldots + \Delta T^n \tag{A-6}$$

where Δr^n and ΔT^n denote the value of Δr and ΔT at the nth iteration.

REFERENCES

1. F. Albrecht, "Untersuchungen über den Wärmehaushalt der Erdatmosphäre und seine thermodynamische Bedeutung," *Berichte des Deutschen Wetterdienstes* in der U.S. Zone, vol. 17, 1950, 70 pp.
2. A. W. Brewer, "Evidence for a World Circulation Provided by the Measurements of Helium and Water Vapor Distribution in the Stratosphere," *Quarterly Journal of the Royal Meteorological Society*, vol. 75, No. 326, Oct. 1949, pp. 351-363.
3. K. Bryan, "Measurements of Meridional Heat Transport by Ocean Currents," *Journal of Geophysical Research*, vol. 67, No. 9, Aug. 1962, pp. 3403-3414.
4. H. S. Buch, "Hemispheric Wind Conditions During the Year 1950." *Final Report*, Part 2, under Contract No. AF 19-122-153, General Circulation Project, Department of Meteorology, Massachusetts Institute of Technology, 1954, 126 pp.
5. M. I. Budyko, "Atlas Teplovogo Balansa Zemnogo Shara," Mezhduvedomstvennyĭ Geofizicheskiĭ Komitet pri Prizidium, Akademiĭa Nauk SSSR, Glavnaĭa Geofizicheskaĭa Observatoriĭa imenniĭ A. E. Voeĭkova, *Rezul'taty*, 1964.
6. M. I. Budyko, *Teplovoĭ Balans Zemnoĭ Poverkhnosti*, Gidrometeorologicheskoe izdatel'stvo, Leningrad, 1956, 255 pp.
7. J. G. Charney and A. Eliassen, "On the Growth of the Hurricane Depression," *Journal of the Atmospheric Sciences*, vol. 21, No. 1, Jan. 1964, pp. 68-75.
8. G. M. B. Dobson, "Origin and Distribution of the Polyatomic Molecules in the Atmosphere," *Proceedings of the Royal Society*, Series A, vol. 236, No. 1205, Aug. 2, 1956, pp. 187-193.
9. H. G. Houghton, "On the Annual Heat Balance of the Northern Hemisphere," *Journal of Meteorology*, vol. 11, No. 1, Jan. 1954, pp. 1-9.
10. J. T. Houghton, "Absorption in the Stratosphere by Some Water-Vapor Lines in the ν_2 Band," *Quarterly Journal of the Royal Meteorological Society*, vol. 89, 1963, pp. 332-338.
11. W. C. Jacobs, "The Energy Exchange Between the Sea and Atmosphere and Some of Its Consequences," *Bulletin of the Scripps Institution of Oceanography*, vol. 6, No. 2, 1951, pp. 27-122.

12. A. Kasahara, "A Numerical Experiment on the Development of a Tropical Cyclone," *Journal of Meteorology*, vol. 18, No. 3, June 1961, pp. 259–282.

13. A. Kochanski, "Cross Sections of the Mean Zonal Flow and Temperature Along 80° W.," *Journal of Meteorology*, vol. 12, No. 2, Apr. 1955, pp. 95–106.

14. H. L. Kuo, "On Formation and Intensification of Tropical Cyclones Through Latent Heat Release by Cumulus Convection," *Journal of the Atmospheric Sciences*, vol. 22, No. 1, 1965, pp. 40–63.

15. C. E. Leith, "Convection in a Six-Level Model Atmosphere," Contract W–7405-eng-48, Lawrence Radiation Laboratory, University of California, Livermore, Calif., 1965.

16. D. K. Lilly, "On the Numerical Simulation of Buoyant Convection," *Tellus*, vol. 14, No. 2, May 1962, pp. 148–172.

17. J. London, "A Study of the Atmospheric Heat Balance," *Final Report* on Contract AF 19(122)–165 (AFCRC–TR–57–287), Department of Meteorology and Oceanography, New York University, 1957, 99 pp.

18. S. Manabe and R. F. Strickler, "On the Thermal Equilibrium of the Atmosphere with a Convective Adjustment," *Journal of the Atmospheric Sciences*, vol. 21, No. 4, July 1964, pp. 361–385.

19. H. J. Mastenbrook, "Frost-Point Hygrometer Measurements in the Stratosphere and the Problem of Moisture Contamination," *Humidity and Moisture* (editor-in-chief A. Wexler), vol. 2 *Applications* (edited by E. J. Amdur), Reinhold Publishing Corp., New York, 1963, pp. 480–485.

20. W. Meinardus, "Eine neue Niederschlagkarte der Erde," *Petermann's Geographische Mitteilungen*, vol. 80, 1934, pp. 1–4.

21. R. J. Murgatroyd, "Some Recent Measurements by Aircraft of Humidity up to 50,000 feet in the Tropics and Their Relationship to Meridional Circulation," *Proceedings of the Symposium on Atmospheric Ozone*, Oxford, *IUGG Monograph* No. 3, Paris, 1959, 30 pp.

22. Y. Ogura, "Frictionally Controlled, Thermally Driven Circulations in a Circular Vortex with Application to Tropical Cyclones," *Journal of the Atmospheric Sciences*, vol. 21, No. 6, Nov. 1964, pp. 610–621.

23. Y. Ogura and J. G. Charney, "A Numerical Model of Thermal Convection in the Atmosphere," *Proceedings of the International Symposium on Numerical Weather Prediction, Tokyo, 1960*, Meteorological Society of Japan, Tokyo, 1962, pp. 431–452.

24. A. H. Oort, "On the Energetics of the Mean and Eddy Circulations in the Lower Stratosphere," *Tellus*, vol. 16, No. 4, 1964, pp. 309–327.

25. K. Ooyama, "A Dynamic Model for the Study of Tropical Cyclone Developments," Department of Meteorology and Oceanography, New York University, 1963, 26 pp.

26. J. P. Peixoto, "Hemispheric Temperature Conditions During the Year 1950," *Scientific Report* No. 4, Contract AF 19 (604)–2242, Department of Meteorology, Massachusetts Institute of Technology, 1960, 142 pp.

27. J. P. Peixoto, "Hemispheric Humidity Conditions During the Year 1950," *Scientific Report* No. 3, Contract AF 19(604)–6108, Department of Meteorology, Massachusetts Institute of Technology, 1958, 211 pp.

28. N. A. Phillips, "Geostrophic Motion," *Reviews of Geophysics*, vol. 1, No. 2, May 1963, pp. 123–176.

29. C. H. B. Priestley, "A Survey of the Stress Between the Ocean and Atmosphere," *Australian Journal of Scientific Research*, series A, vol. 4, No. 3, Sept. 1951, pp. 315–328.

30. B. Saltzman, "Spectral Statistics of the Wind at 500 mb," *Journal of the Atmospheric Sciences*, vol. 19, No. 2, Mar. 1962, pp. 195–206.

31. J. Smagorinsky and G. O. Collins, "On the Numerical Prediction of Precipitation," *Monthly Weather Review*, vol. 83, No. 3, Mar. 1955, pp. 53–68.

32. J. Smagorinsky, "On the Inclusion of Moist Adiabatic Processes in Numerical Prediction Models," *Berichte des Deutschen Wetterdienstes*, Band 5, Nr. 38, 1956, pp. 82–90.

33. J. Smagorinsky, "On the Dynamical Prediction of Large-Scale Condensation by Numerical Methods," "Physics of Precipitation", *Geophysical Monographs*, No. 5, American Geophysical Union, 1960, pp. 71–78.

34. J. Smagorinsky, "A Primitive Equation Model Including Condensation Processes," *Proceedings of the International Symposium on Numerical Weather Prediction in Tokyo, 1960*, Meteorological Society of Japan, Mar. 1962, p. 555.

35. J. Smagorinsky, S. Manabe, and J. L. Holloway, "Numerical Results From a Nine-Level General Circulation Model of the Atmosphere," *Monthly Weather Review*, vol. 93, No. 12, Dec. 1965, pp. 727–768.

36. J. Smagorinsky and Staff Members, "Prediction Experiments with a General Circulation Model," *Proceedings of the International Symposium on Dynamics of Large-Scale Processes in the Atmosphere (IAMAP/WMO), Moscow, USSR*, 1965.

37. Staff Members of Tokyo University, "The Quantitative Forecast of Precipitation with the Numerical Prediction Method," *Journal of Meteorological Society of Japan*, Series 2, vol. 33, No. 5, 1955, pp. 25–36.

38. V. P. Starr and R. M. White, "Balance Requirements of the General Circulation," *Final Report*, Part I, Contract AF 19(122)–153, Department of Meteorology, Massachusetts Institute of Technology, 1954, pp. 186–242.

39. K. Telegadas and J. London, "A Physical Model of the Northern Hemisphere Troposphere for Winter and Summer," *Scientific Report* No. 1, Contract AF 19(122)–165, Research Division, College of Engineering, New York University, 1954, 55 pp.